Article:

Refiei, A, Loni, R, Najafi, G et al. (3 more authors) (2020) 4E assessment of power generation systems for a mobile house in emergency condition using solar energy: a case study. Journal of Thermal Analysis and Calorimetry. ISSN 1388-6150

https://doi.org/10.1007/s10973-020-10193-0

4E Assessment of Power Generation Systems for a Mobile House in Emergency Condition such as Earthquake using Solar Energy: A Case Study, Kermanshah, Iran.

Reyhaneh Loni[a], G. Najafi[a,*], Evangelos Bellos[b], D. Wen[c,d]

[a] Department of Biosystem Engineering, Tarbiat Modares University, Tehran, Iran.
[b] Thermal Department, School of Mechanical Engineering, National Technical University of Athens, Greece.
[c] School of Aeronautic Science and Engineering, Beihang University, Beijing, China.
[d] School of Chemical and Process Engineering, University of Leeds, Leeds, UK

***Corresponding Author:** g.najafi@modares.ac.ir, Tel: +98-912 366 4393

Abstract

In this study, a solar Parabolic Trough Concentrator (PTC) was evaluated as heat source of a power generation system based on energy (E1), exergy (E2), environmental (E3), and economic (E4) analyses. Different configurations of power generation system were investigated including solar Steam Rankine Cycle (SRC), solar Organic Rankine Cycle (ORC), and solar SRC-ORC system. Water, and R113 were used as working fluids of SRC, and ORC system, respectively. It should be mentioned that the proposed solar systems were evaluated for providing required power of a mobile-house in emergency condition such as earthquake that was happened in Kermanshah, Iran, on 2016 with many homeless people. The PTC system was optically and thermally investigated based on sensitivity analysis. The optimized solar PTC system was studied as heat source of the Rankine cycle with three different configurations for power generation. Then, the solar Rankine cycle systems were investigated based on 4E analyses for providing power of the mobile-house based on different numbers of solar RC units. It was concluded that the combined solar SRC+ORC system can be recommended for achieving the highest 4E performance. It was resulted that decreasing condenser temperature, increasing energy and exergy performance. On the other side, optimum TIT of 499 K was calculated for the ORC system for achieving the highest 4E

performance. The highest total energy efficiency, and exergy electrical efficiency of the optimized power system were calculated as 40.44%, and 43.36%, respectively.

Keywords: 4E analyses; Solar Steam Rankine Cycle (SRC); Solar Organic Rankine Cycle (ORC); Combination of solar SRC and solar ORC; Designing a mobile-house for natural disasters.

Nomenclature

A	Area, m^2
c_p	Constant pressure specific heat, J/kgK
d	Inner diameter (m)
D	Outer diameter (m)
h	Convection heat transfer coefficient, W/m^2K
h^*	Enthalpy, kJ/kg
$\acute{h}$	Internal heat transfer coefficient, W/m^2K
I_{sun}	Solar irradiance (W/m^2)
k_{ab}, K	Thermal conductivity, W/mK
$\dot{m}$	System mass flow rate, kg/s
Nu	Nusselt number,-
Pa	Absolute pressure at annular (mmHg)
Pr	Prandtl number
Pr_w	Prandtl number at the wall temperature
q	Incident heat transfer flow per length at a boundary (W/m)
$\dot{Q}_{net}$	Net heat transfer rate, W
$\dot{Q}^*$	Rate of available solar heat at receiver, W
$\dot{Q}_{loss}$	Loss rate of heat loss from the receiver, W
R	Thermal resistance, K/W
Ra	Rayleigh number
Re	Reynolds number,-
T	Temperature, K
T_a	Temperature at a boundary (°C)
T_{dew}	Dew point (°C)
T_{oo}	Ambient temperature (°C)
$\overline{\Delta T}_{ab}$	Temperature difference between a and b boundaries (°C)
$\dot{W}$	Power, W

Greek symbols

γ	Specific heat ratio
δ	Molecular diameter of annular gas (cm)
ε_α	Emittance at a boundary
η	Efficiency, -
ρ	Density, kg/m^3
σ	Stefan-Boltzmann constant, [$=5.67\cdot10^{-8}$ W/m^2K^4]

Subscripts

0	*initial inlet to receiver*
ap	*aperture*
ab	*absorber*
c	*condenser*
cond	*due to conduction*
conv	*due to convection*
cr	*critical*
evp	*evaporator*
f	*fluid*
II	*second law of thermodynamic*
inlet	*at the inlet*
n	*receiver section number*
net	*net*
optical	*optical*
overall	*overall*
P	*pump*
ref	*reflector*
rad	*due to radiation*
s	*surface of the inner tube*
T	*turbine*

th	*thermal*
total	*total*
amb, air	*environment*

Abbreviations

AST	Archimedes Screw Turbine
ORC	Organic Rankine cycle
PTC	Parabolic Trough Concentrator
SRC	Steam Rankine Cycle

1 Introduction

Nowadays, renewable energies are accounted as alternatives for fossil fuels for providing our energy security [1]. Environmental pollution can be reduced by the use of renewable energies [2]. There are different renewable energies such as solar, wind, geothermal, and wave energies. Generally, solar energy is one of the most promising energy forms [3]. Solar collectors are used for converting solar energy to thermal energy of solar working fluids [4]. Parabolic trough Concentrators (PTCs) are accounted as interesting and world-wide concentrating collectors.

There have been extensive studies related to the performance of PTC systems with evacuated tube receiver. Song et al. [5] developed a method for calculating heat flux distribution of a PTC system. They found there is a good agreement between the presented method and traditional 3D ray-tracing methods. Time of calculation was reduced from the 40s to 0.22s based on the proposed method. Jaramillo et al. [6] investigated PTC systems for achieving hot water based on experimental tests. The PTCs were constructed based on two rim angles including 45º, and 90º. They found the PTC with rim angle of 90º showed higher efficiency compared to the one with rim angle of 45º. Bellos and Tzivanidis [7] reviewed the design of PTC systems with higher performance and lower cost for different applications. Azzouzi et al. [8] experimentally investigated a PTC system with large rim angle and presented steps of building the PTC in detail. Khanna et al. [9] investigated the thermal stress of a bimetallic receiver as the absorber of a PTC system. Thermal stress was considered under the non-uniform temperature of the receiver. Some relationships were developed for the prediction of the thermal stress in the receiver of the PTC system.

Caldiño-Herrera et al. [10] studied a solar PTC system as a heat source of an ORC system. Performance of the system was estimated based on the first and second laws of thermodynamics. R245fa was used as the ORC working fluid. Wirz et al. [11] simulated a PTC system with different coating for improving the optical performance of the solar system. They investigated different properties of solar reflector such as reflectivity, tracking error, and optical errors. They found that thermal efficiency had increased up to 23% based on the optimized PTC system. Karathanassis et al. [12] evaluated a solar system including PTC and PV experimentally. Thermal and electrical efficiency of the system were measured as 44%, and 6%, respectively. They found the efficiency of the system was dependent on the optical properties of the CPVT system. Srivastava and Reddy [13] considered a PTC system with PV technology under thermal and electrical aspects. A CPC system was used as a secondary reflector for providing uniform heat flux. Aluminum/water nanofluid was used as the solar working fluid. They found that the thermal performance of the system increased by application of nanofluid, whereas the electrical performance of the system decreased by using nanofluid. Kincaid et al. [14] considered the optical performance of three different types of solar concentrator including the solar tower, Fresnel, and PTC systems. The receiver of the solar towers was determined as a sensitive solar system to the optical errors of the reflectors. On the other hand, the PTC system was introduced as the highest optical efficiency compared to other investigated solar systems.

On the other side, Rankine cycles are suggested as an effective technology for power generation [15, 16]. Dincer and Demir [17] presented Rankine cycles using steam and organic fluids in detail. Aboelwafa et al. [18] reviewed solar Rankine cycle as an effective system for power generation. Garg et al. [19] compared the performance of a Rankine cycle for power generation using CO_2 and steam as the Rankine cycle working fluid. Solar concentrators were investigated as the heat source. The Rankine cycle with CO_2 resulted in lower sensitivity to the heat source temperature compared to the application of steam as the working fluid. Also, Cheang et al. [20] economically compared Rankine cycle using superheated CO_2, and steam as the Rankine cycle working fluid. Solar concentrator collector was used as the heat source. Steam Rankine cycle resulted in higher efficiency compared to the superheated CO_2 Rankine cycle. Li et al. [21] studied a power generation system using a combination of steam Rankine cycle, and an organic Rankine cycle. PTC systems were used as the heat source. The efficiency of the suggested system was calculated from 13.68% to 15.62%. In another study, Li et al. [22] investigated a solar power system using a Rankine cycle. Steam and organic Rankine cycles were used for power generation, whereas PTC systems were used for absorbing solar energy. Optimum conditions of the system were determined.

Sarmiento et al. [23] considered a power generation system using solar energy. They considered a Rankine cycle with a PTC system under energy, exergy, and exergoeconomic aspects. The optimum dimensions of the system were determined. Morrone et al. [24] considered a power generation system using an organic Rankine cycle. Combination of solar energy and biomass was used as the ORC heat source. The combination heat source showed higher global efficiency. Bouvier et al. [25] experimentally investigated a CHP system for producing heat and power using solar energy. A PTC system was used for absorbing solar energy, whereas a steam Rankine cycle was used for power generation. They found that the electrical efficiency was calculated to equal to 3% based on the experimental tests. Carlson et al. [26] developed a power generation system using a Rankine cycle. An unclear power plant was used as the Rankine cycle heat source. Effect of thermal energy storage was thermodynamically investigated in this research. Pelay et al. [27] evaluated a Rankine cycle for power generation using solar concentrator systems as the Rankine cycle heat source under energy and exergy aspects. Thermal energy storage was used in the suggested system. Mohammadi and McGowan [28] investigated a solar steam Rankine cycle as a multi-generation system. The solar tower was used as the Rankine cycle heat source. They found the steam at lower temperature and higher pressure resulted in higher efficiency. Shaaban [29] optimized solar steam and organic Rankine cycle for power generation. They found R1234ze(z) was determined as the organic fluid for achieving the highest performance.

Also, some other researchers investigated on 4E analyses of the ORC systems. Shayesteh et al. [30] investigated on 4E analyses of an ORC system which was combined with a RO system for generation power and freshwater. Different parameters were optimized using genetic algorithm method. Based on three parameters optimization, it was found that R245ca was the best organic working fluid. Wang et al. [31] evaluated 4E analyses of a solar-assisted CCHP system for generation power, heat, and cool. Parabolic Trough Concentrator (PTC) was used for absorbing solar energy, whereas, Brayton cycle were used for power generation. They found that the energy and exergy efficiencies are reported equal to 83.6% and 24.9%, respectively.

As seen from the mentioned literature review, 4E analysis of a solar Rankine cycle with different configurations of power generation system is investigated as a new subject for research. In this study, solar PTC with different configurations of power generation system was investigated including solar SRC, solar ORC, and solar SRC-ORC system. The suggested solar systems were evaluated based on energy (E1), exergy (E2), environmental (E3), and economic (E4) analyses. It should be mentioned that the proposed solar systems were evaluated for providing required power of a mobile-house in emergency condition such as earthquake that was happened in Kermanshah, Iran, on 2016 with many homeless people. In the first step, the PTC system was optically and thermally investigated based on sensitivity analysis for determining the best position of the PTC receiver, and optimum diameter of the vacuum tube receiver. In the next step, the optimized solar PTC system was investigated as heat source of the Rankine cycle with three different configurations for power generation. Then, the solar Rankine cycle systems were environmentally and economically investigated for providing power of the mobile-house based on different numbers of solar RC units. Finally, it should be mentioned that this study was conducted for presenting a solar system for providing required power of homeless people in natural disasters such as Kermanshah earthquake on 2016 that Iran government faced many problems.

2 Modeling and Description

2.1 Case Study

An earthquake with a moment magnitude of 7.3 occurred on the Iran–Iraq border at 34° 54′ 18″ N, 45° 57′ 21.6″ E on 12 November 2016 at 18:18 UTC (21:48 Iran Standard Time) [32]. A view of the earthquake location has been presented in Figure 1. The earthquake was close to the Iraqi Kurdish city of Halabja, and the Kurdish dominated places of Ezgeleh, Salas-e Babajani County, Kermanshah Province in Iran [32]. This was the strongest earthquake recorded in the region since a 6.1 M_w event in January 1967 with at least 630 people killed, more than 8,100 injured, and more than 70,000 homeless [32]. Some scenes of the earthquake have been displayed in Figure 2.

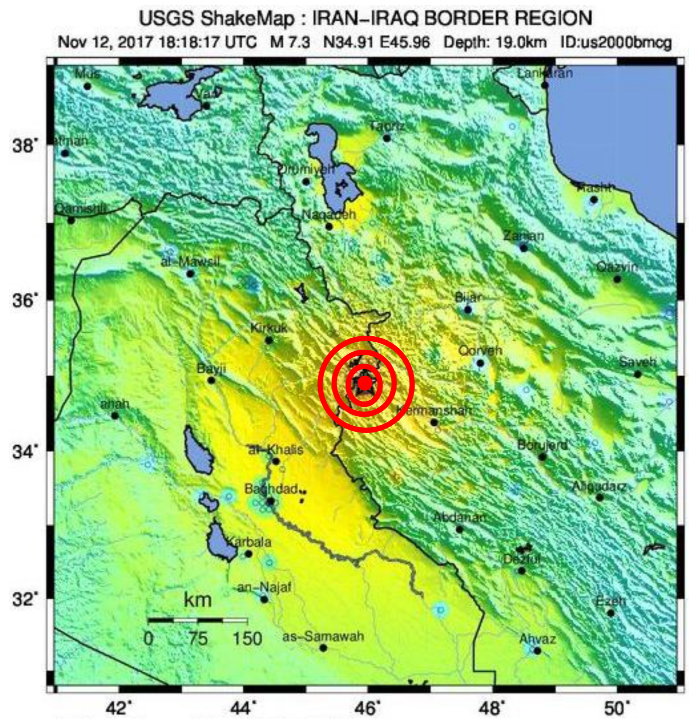

Figure 1: A map of an earthquake with a moment magnitude of 7.3 occurred on the Iran–Iraq border on 12 November 2017.

Figure 2: Some scenes of the earthquake on the Iran–Iraq border on 12 November 2017.

As mentioned, more than 70000 people had been homeless. Consequently, designing some mobile houses are sessional for similar condition that can be established very soon with self-power-generation. It is most prefect, designing some mobile house with generation required power using renewable energy such as solar energy. In the current research, a mobile house was evaluated with generation power by the solar energy. Figure 3 presents a plot of the mobile house for emergency condition such as earthquake. A list of used devices of the mobile house was presented in Table 1. Five light bulbs, one television, and one refrigerator with required power as reported in Table 1.

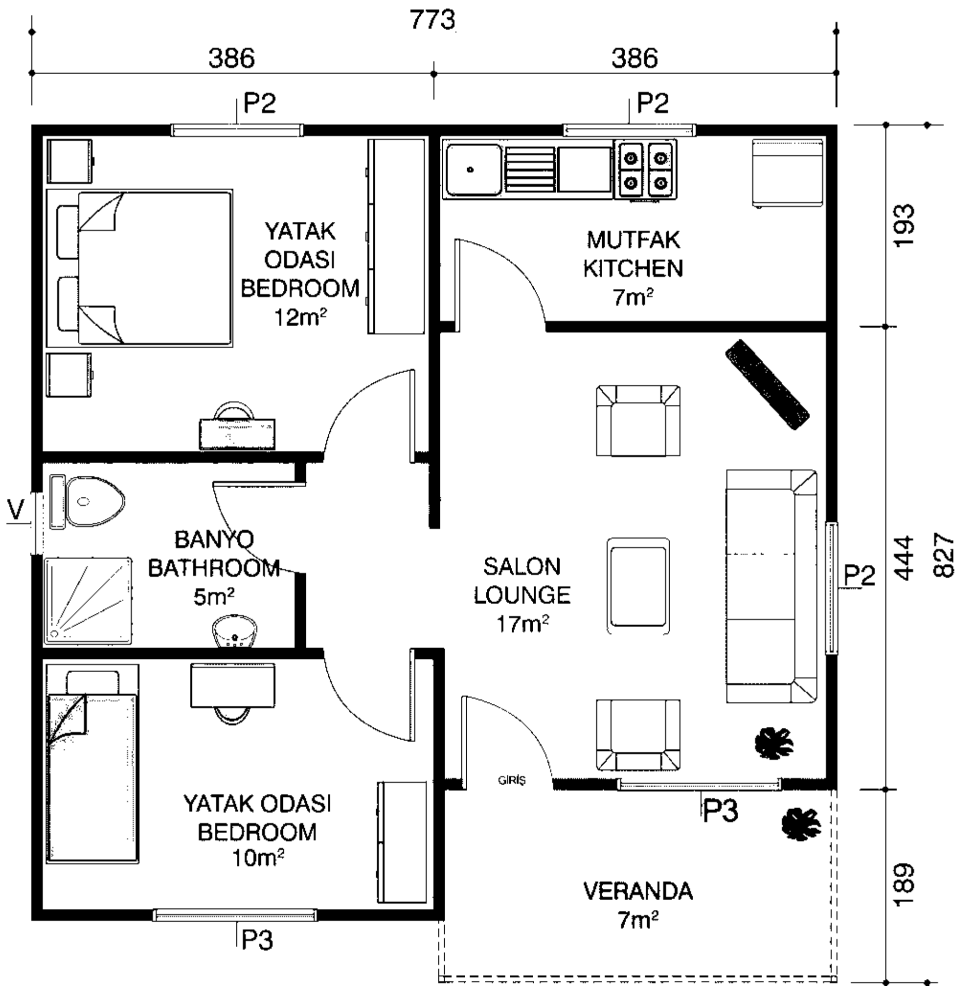

Figure 3: Plot of the mobile house for emergency condition such as earthquake.

Table 1: A list of used devices in the investigated building.

Device	Number	Duration used per day	Required power per day (Wh/day)
Light bulb	5 (10 W)	8 h	400
Refrigerator A^+	1	24 h	1500
TV	1	5 h	800

2.2 Solar System

A schematic of the investigated solar system is depicted in Figure 4. A conventional receive with a glass cover was investigated. All of the incoming solar radiation at the PTC aperture will be concentrated at the PTC focal line, where the receiver is located. Dimensions of the solar PTC were presented in [33] The optical simulation of the solar system was done using SolTrace software. The SolTrace software is recommended as a free and efficient software for optical modeling of concentrator systems [4, 34]. On the other side, the thermal modeling of the solar system was numerically conducted in Maple software. Energy balance equations were used for thermal modeling.

Table 2: Dimensions of steel mirror reflector.

Parameters	Values
Parabola length (L_c)	2 m
Parabola aperture (w)	70 cm
Focal distance (f)	17.5 cm
Thickness (mean value)	0.8 mm

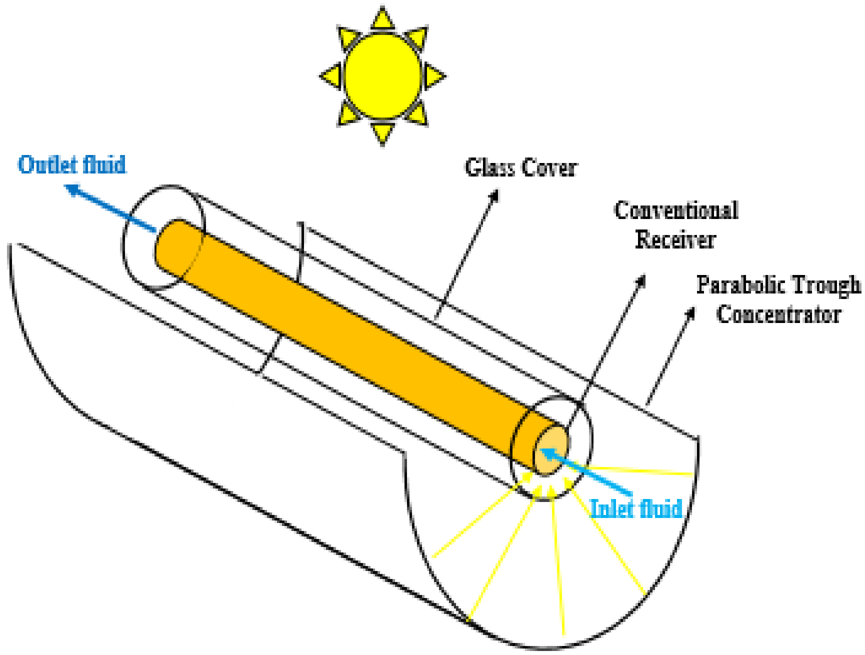

Figure 4: A schematic of the PTC system with a conventional receiver.

2.3 Power Generation System

In this section, the solar PTC system was used as a heat source of power generation cycles. Three different scenarios were assumed for power generation including SRC, ORC, and combination of SRC and ORC systems. A schematic view of the investigated SRC, ORC, and combination of SRC and ORC systems for power generation is presented in Figure 5a, 5b, and 5c, respectively. It should be mentioned that water and R113 were selected as working fluids of the SRC, and ORC systems, respectively.

As shown in Figure 5, the Rankine cycles are consists of an evaporator that steam absorbs heat, a turbine that generates power, a condenser for phase changing the steam to water, and a pump for circulating steam-water in the Rankine cycle. Figure 6 shows a T-S diagram of water as the working fluid of the Rankine cycle. In this cycle, water is pressurized in the pump under isentropic condition based on the process of 1-2 in Figure 6. Then, the pressurized water is entered in the evaporator for absorbing heat and converting to the saturated or superheated fluid under constant pressure under the process of 2-3 in Figure 6. The saturated or superheated steam generates power in the turbine at the isentropic condition under the process of 3-4 on Figure 6.

Finally, the exiting fluid from the turbine is cooled in the condenser under constant pressure under the process of 4-1 in Figure 6. It should be mentioned that the Rankine cycles were investigated under at constant evaporator pressure of 3 MPa and the condenser temperature of 311 K.

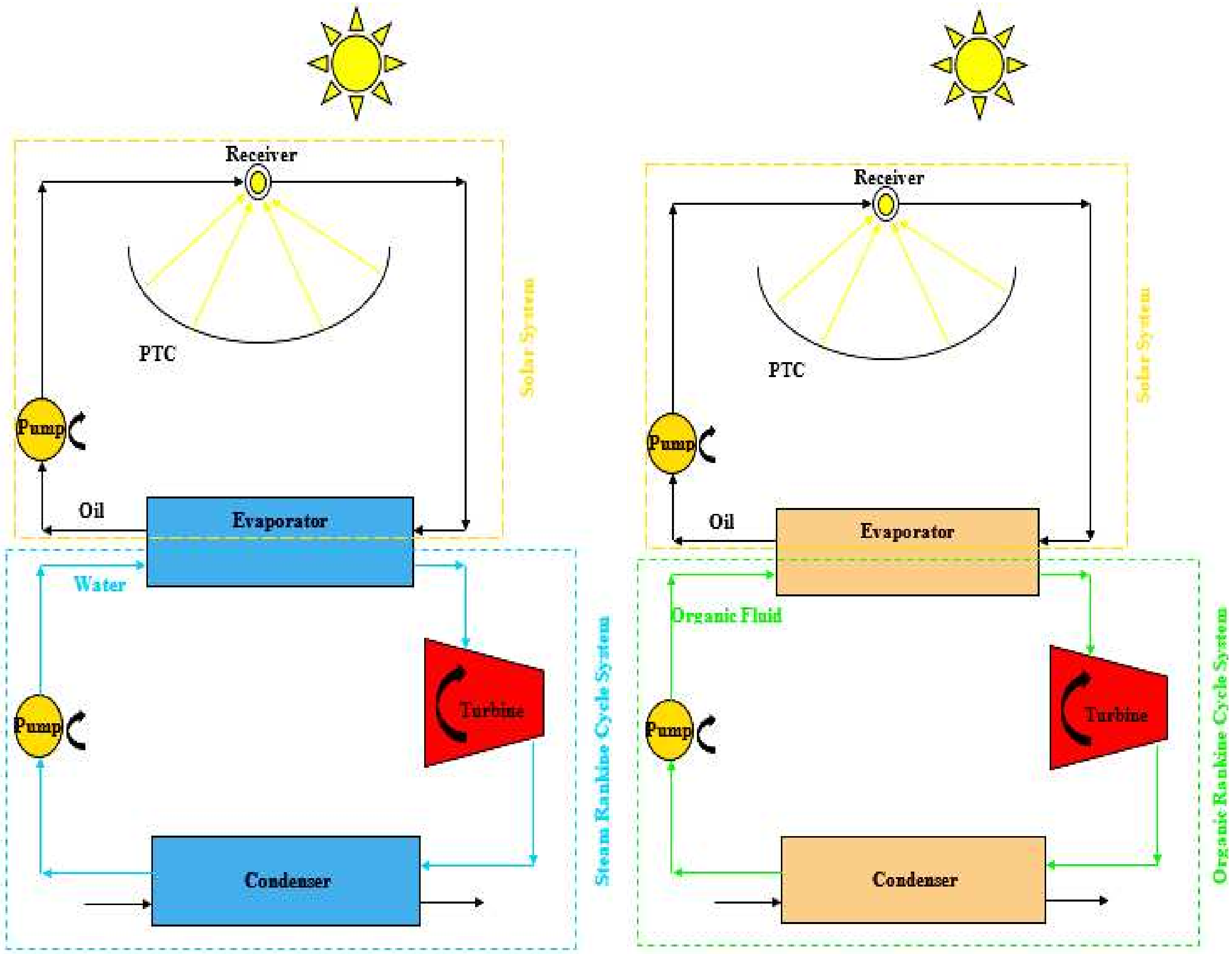

(a) (b)

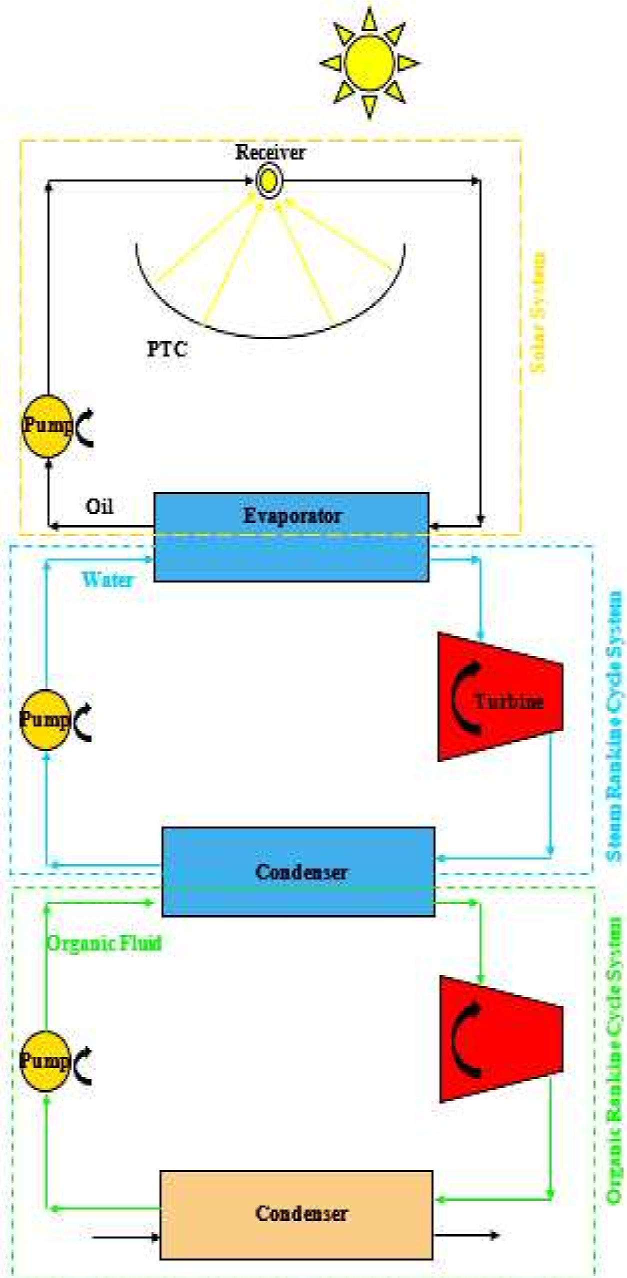

(c)

268 **Figure 5: Different scenarios for power generation cycles including: a) SRC, b) ORC, and c) combination**
269 **of SRC and ORC.**

270

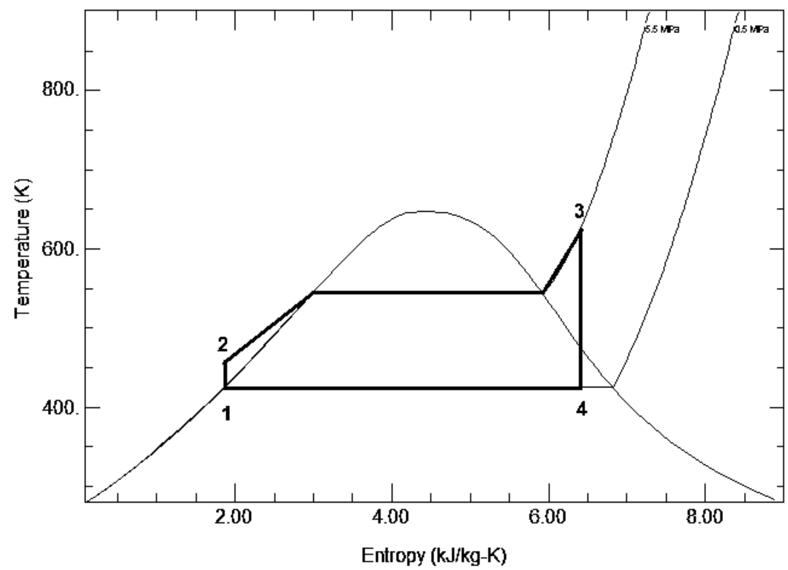

Figure 6: T-S diagram of water as the working fluid of the Rankine cycle.

2.4 Energy Analysis

As mentioned the optical modeling was done using the SolTrace software. A view of the PTC optical modeling using the SolTrace software was presented in Figure 7. The optical analysis was done for five levels of the optical error as 5 mrad, 10 mrad, 15 mrad, 20 mrad, and 35 mrad, and three levels of the tracking error as 0º, 1º, and 2º. The position of the receiver compared to the focal line was optimized during the optical investigation. Also, the solar system was optically considered under variation of PTC aperture area. Table 3 presents constant assumed parameters for optical modeling using the SolTrace software.

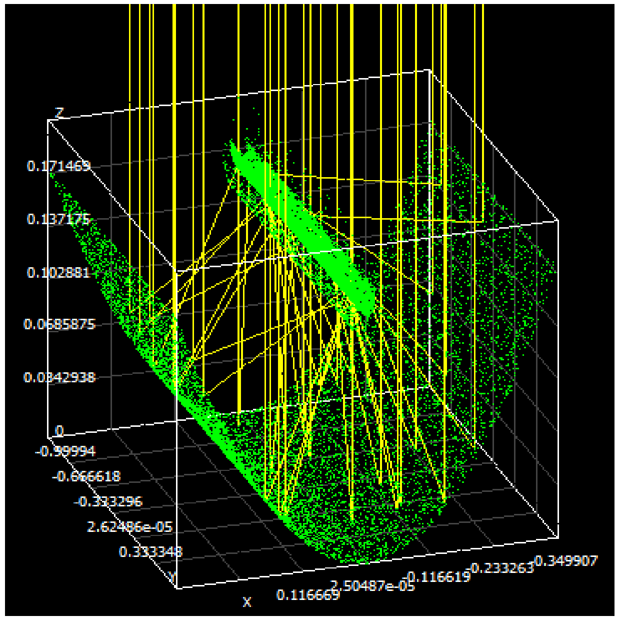

Figure 7: A view of the PTC optical modeling in SolTrace.

Table 3: SolTrace modeling assumed constants.

Parameter	Assumed constant
The sun-shape	pillbox
The half-angle width	4.65 mrad
Number of ray intersections	10000
The reflectance of the cavity walls (black cobalt coating)	15%

Another part of this study is the thermal modeling of the investigated solar system. The PTC system with the conventional receiver was thermally modeled based on energy balance equations as mentioned previous. The net absorbed heat by the receiver was calculated based on the heat gain that was assumed by the SolTrace, and receiver heat losses. A schematic of the receiver heat losses was presented in Figure 8.

The receiver heat losses were calculated using the thermal resistance method. A view of the thermal resistance method that was used in this study is presented in Figure 9. As seen from Figure 9b, the receiver heat losses are including annual radiation and convection heat losses, conduction heat losses form the glass cover, and radiation and convection heat losses. Thermal heat losses from the receiver will be explained in detail in the next paragraphs.

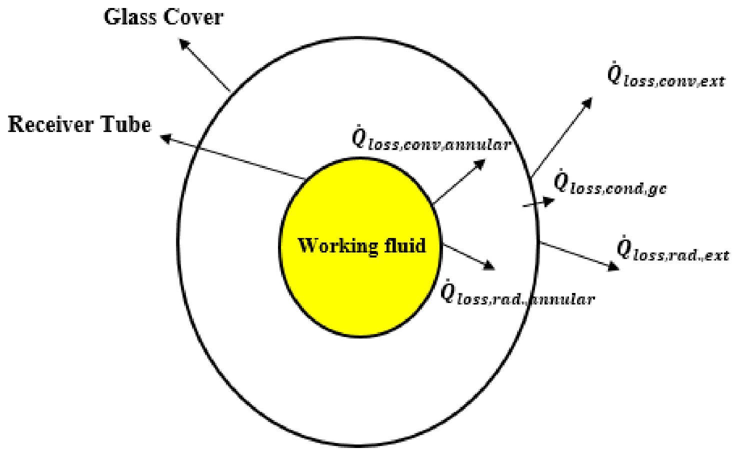

Figure 8: Schematic of the receiver heat losses.

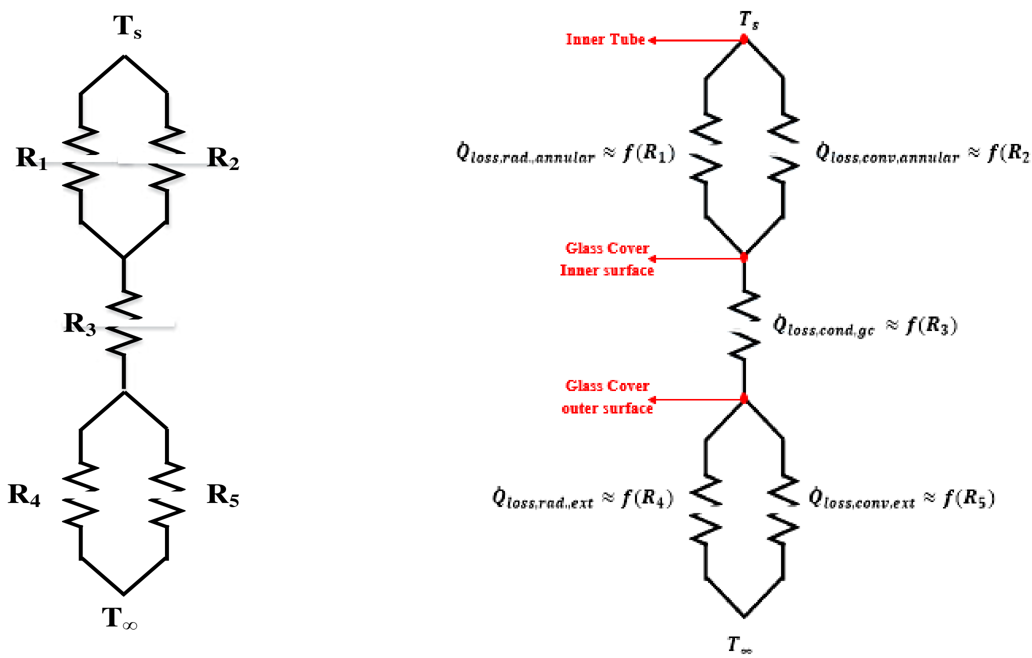

(a) **(b)**

Figure 9: A schematic of the a) thermal resistance method, and b) heat losses from the receiver.

As mentioned, a part of the receiver heat losses is including the annular convection and radiation heat losses. Natural convection heat losses in the vacuumed space between the receiver tube, and glass cover can be calculated as following [35]:

$$h_1 = \frac{1}{\left(\frac{D}{2}\right)\ln\left(\frac{d}{D}\right) + \left(\frac{9\gamma - 5}{2(\gamma + 1)}\right)\left(2.331 \times 10^{-20}\,\frac{\bar{T}_{23} + 237}{P_a \delta^2}\right)\left(\frac{d}{D} + 1\right)} \tag{1}$$

Whereas the radiation heat losses from the vacuumed space between the receiver tube, and glass cover can be calculated as below [36]:

$$\acute{q}_2 = \frac{\sigma \pi D (T_D^4 - T_d^4)}{\frac{1}{\varepsilon_d} + \frac{D(1 + \varepsilon_D)}{d \varepsilon_D}} \tag{2}$$

As seen in Figure 9b, another heat loss of the PTC receiver is caused by conduction heat losses from the glass cover. The conduction heat losses from the glass cover can be estimated by the bellow equation [36]:

$$\acute{q}_3 = 2\pi k_{45} \frac{\Delta T_{45}}{ln \frac{D_5}{D_4}} \tag{3}$$

- <u>Natural External Convection</u>

  The Nusselt number of the natural external convection of the PTC receiver can be calculated as below [37]:

$$Nu_{4,natural} = \left[0.6 + \frac{0.378\, Ra^{1/6}}{\left(1 + \left(\frac{0.599}{Pr}\right)^{9/16}\right)^{8/27}}\right]^2 \tag{4}$$

- <u>Cross-flow External Forced Convection</u>

The Nusselt number of the cross-flow external forced convection of the PTC receiver can be defined as following [38]:

$$Nu_{4,forced} = cRe^m Pr^n \left(\frac{Pr}{Pr_w}\right)^{1/4} \tag{5}$$

Consequently, the total Nusselt number of the external heat losses from the PTC receiver due to the natural and forced convection can be calculated as following [39]:

$$Nu_{4,total} = \left(Nu_{natural}{}^{3.5} + Nu_{forced}{}^{3.5}\right)^{1/3.5} \tag{6}$$

- <u>External Radiation</u>

The external radiation heat losses from the PTC receiver can be calculated as below [40]:

$$\acute{q}_5 = \sigma\varepsilon\pi D(T_D^4 - T_{ci}^4) \tag{7}$$

Where

$$T_{ci} = T_\infty \sqrt[4]{\varepsilon_{ci}} \tag{8}$$

$$\varepsilon_{ci} = 0.711 + 0.56\frac{T_{dew}}{100} + 0.73\left(\frac{T_{dew}}{100}\right)^2 \; ; \; T_{dew} = [°\mathrm{C}] \tag{9}$$

Based on the presented equations, and using thermal resistance approach, the total thermal resistance of the system can be calculated as below [39]:

$$R_{total} = R_{total,1} + R_3 + R_{total,2} \tag{10}$$

Where $R_{total,1}$ is defined as thermal resistance of the PTC receiver between the absorber tube and the cover glass in an annual region. $R_{total,2}$ is defined as the thermal resistance from the PTC receiver to the environment. Finally, R_3 is thermal resistance of the PTC receiver due to the glass cover conductivity. $R_{total,1}$, and $R_{total,2}$ can be calculated as following:

$$R_{total,1} = \frac{R_1 \times R_2}{R_1 + R_2} \tag{11}$$

$$R_{total,2} = \frac{R_4 \times R_5}{R_4 + R_5} \tag{12}$$

In this equation, $\dot{Q}_{net,total}$ is total absorbed heat by the PTC receiver. Total absorbed heat can be calculated by solving Eqs. **(13)** and **(14)** simultaneously using the Newton–Raphson Method [39]:

$$\dot{Q}_{net,n} = \dot{Q}^*{}_n - \frac{A_n}{R_{total}}(T_{s,n} - T_{amb}) \tag{13}$$

And

$$\dot{Q}_{net,n} \quad = \frac{(T_{s,n} - \sum_{i=1}^{n-1}\left(\frac{\dot{Q}_{net,i}}{\dot{m}\ c_{p0}}\right) - T_{inlet,0})}{(\frac{1}{\hbar A_n} + \frac{1}{2\ \dot{m}\ c_{p0}})} \tag{14}$$

Where,

$$\hbar = \frac{Nu_{inner} K_{fluid}}{d_{tube}} \tag{15}$$

$$Nu_{inner} = \frac{\left(\frac{f_r}{8}\right).Re.Pr}{1 + 12.8.\sqrt{\frac{f_r}{8}}.(Pr^{0.68} - 1)} \tag{16}$$

$$f_r = (0.79\, ln\, Re - 1.64)^{-2} \tag{17}$$

The thermal efficiency of the solar PTC system is defined as the absorbed solar heat by the PTC receiver to the incoming solar radiation to the PTC aperture. The thermal efficiency can be calculated as follows:

$$\eta_{th} = \frac{\dot{Q}_{net,total}}{\dot{Q}_{\ solar}} = \frac{\sum_{n=1}^{N} \dot{Q}_{net,n}}{I_{sun} A_{ap,PTC}} \tag{18}$$

It should be mentioned that Behran thermal oil was used as the solar working fluid, whereas thermal properties of the thermal oil were used based on ref. [4].

About power generation cycles, the mass flow rate of the Rankine cycle working fluid was calculated based on the following equation [41]:

$$\dot{m}_{RC} = \frac{\dot{Q}_{evp}}{(h^*{}_3 - h^*{}_2)} \tag{19}$$

Where, $\dot{Q}_{evp}$ (W) is absorbed solar energy by the receiver that transferred to the water in the evaporator. The generated power by the turbine can be calculated using Eq. (**20**) [41].

$$\dot{W}_T = \dot{m}_{RC}(h^*{}_3 - h^*{}_4) \tag{20}$$

The ejected heat by the condenser can be calculated using Eq. (**21**) [41]:

$$\dot{Q}_c = \dot{m}_{RC}(h^*{}_4 - h^*{}_1) \tag{21}$$

The consumed energy by the pump for circulation water-steam in the Rankine cycle can be calculated as [41]:

$$\dot{W}_P = \dot{m}_{RC}(h^*{}_2 - h^*{}_1) \tag{22}$$

The net generated power by the Rankine cycle can be calculated as [41]:

$$\dot{W}_{net} = \dot{W}_T - \dot{W}_P = \dot{m}_{RC}[(h^*{}_3 - h^*{}_4) - (h^*{}_2 - h^*{}_1)] \tag{23}$$

Finally, the Rankine cycle efficiency and overall efficiency of the solar Rankine cycle can be calculated using Eqs. **(24)** and **(25)**, respectively.

$$\eta_{RC} = \frac{\dot{W}_{net}}{\dot{Q}_{evp}} \tag{24}$$

$$\eta_{overall} = \frac{\dot{W}_{net}}{I_{beam} \cdot A_{ap,dish}} \tag{25}$$

2.5 Exergy Analysis

Exergy analysis is introduced as a useful tool for prediction of the maximum available useful work during a process that brings the system into equilibrium with environmental. Exergy value of the sun can be defined as below, where T_{sun} was assumed equal to 5800 K [41]:

$$Ex_{Sun} = I_{sun}\, A_{aperture,PTC}\left[1 - \frac{4}{3} \cdot \frac{T_{amb}}{T_{sun}} + \frac{1}{3}\left(\frac{T_{amb}}{T_{sun}}\right)^4\right] \tag{26}$$

Finally, exergy electrical efficiency can be defined as:

$$\eta_{overall} = \frac{\dot{W}_{net}}{Ex_{Sun}} \tag{27}$$

2.6 Economic Analysis

Economic analysis is introduced as a useful tools for determining more efficient method for power generation between the suggested scenarios in the current research. There are different economic parameters including Levelized Cost of Electricity (LCOE), Cash Flow (CF), and Simple Payback Period (SPP). Amount of LCOE, CF, and SPP parameters can be defined as:

$$LCOE = \frac{I_t + M_t + F_t}{E_t} \tag{28}$$

$$CF = \left[E_{t,yearly} * C_{el}\right] - M_t \tag{29}$$

$$SPP = \frac{I_t}{CF} \tag{30}$$

Where

$$I_t = I_{t,PTC} + I_{t,ORC} \tag{31}$$

$$M_t = 0.01 \cdot N \cdot I_t \tag{32}$$

$$E_t = N \cdot E_{t,yearly} \tag{33}$$

In these equations, I_t (€) is defined as value of investment cost, M_t (€) is defined as amount of maintenance cost, F_t (€) is defined as value of the cost of fossil fuel that it assumed equal to zero in this study, E_t(kWh) is defined as values of generated power, $I_{t,PTC}$ is defined as amount of the investment cost of the solar PTC system that was assumed 275 €/m^2 [43], $I_{t,ORC}$ is defined as value of the investment cost of the ORC system that was assumed 3000 €/kWh [43], N is value of the estimated lifetime of the solar ORC system that was assumed equal to 25 years in this research, $E_{t,yearly}$ (kWh) is yearly generated power by the solar ORC system, and C_{el} (€/kWh) is defined as amount of the financial value of electricity produced which was assumed equal to 0.2 in this study [43].

2.7 Environmental Analysis

The environmental influence of different sources of energy is introduced as an essential parameter for selecting the source of energy. Application of renewable energy, including solar energy as a source of the required energy, is accounted as an exciting way of reducing CO_2 emission. In the current study, CO_2 mitigated per annum, and carbon credit was calculated for the solar HDD-ORC system. Also, the influence of different nanofluids as the solar working fluid will be investigated on environmental parameters. The CO_2 mitigated per annum can be estimated as [42]:

$$\varphi_{CO_2} = \frac{\psi_{CO_2} \times E_{en,ann}}{10^3} \quad \textbf{(34)}$$

Where, φ_{CO_2} (tone) is CO_2 emission per annum, ψ_{CO_2} (kgCO_2/kWh) is average CO_2 producing for power generation from coal that was assumed equal to 2.04, and $E_{en,ann}$(kWh) is power generation by the solar or ORC systems during a year, whereas each year was assumed 2500 hr for Tehran, Iran as a case study. Also, carbon credit (Z_{CO_2}) can be calculated as below [42]:

$$Z_{CO_2} = z_{CO_2} \times \varphi_{CO_2} \quad \textbf{(35)}$$

Where Z_{CO_2}($) is carbon credit per annum, z_{CO_2}($/ton) is carbon credit which was assumed equal to 14.5, and φ_{CO_2}(ton) is CO_2 emission per annum [42].

2.8 Validation of the developed model

Thermal performance of the solar PTC system with the vacuum tube receiver was validated based on the experimental results of a built PTC collector in Tehran University, Tehran, Iran [44]. A view of the experimental setup is presented in Figure 10. Figure 11 presents a comparison between the measured global efficiency by Reference [38] and the calculated numerical results in the current study. There is good agreement between the experimental results and the calculated results in this research.

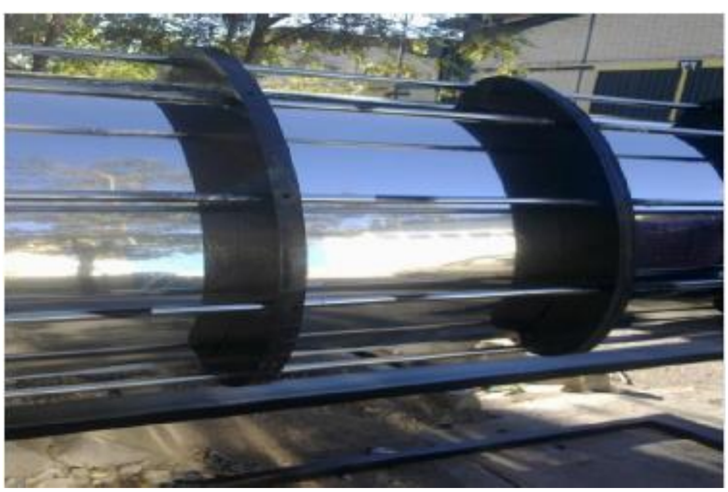

Figure 10: Investigated the PTC system by Reference [44].

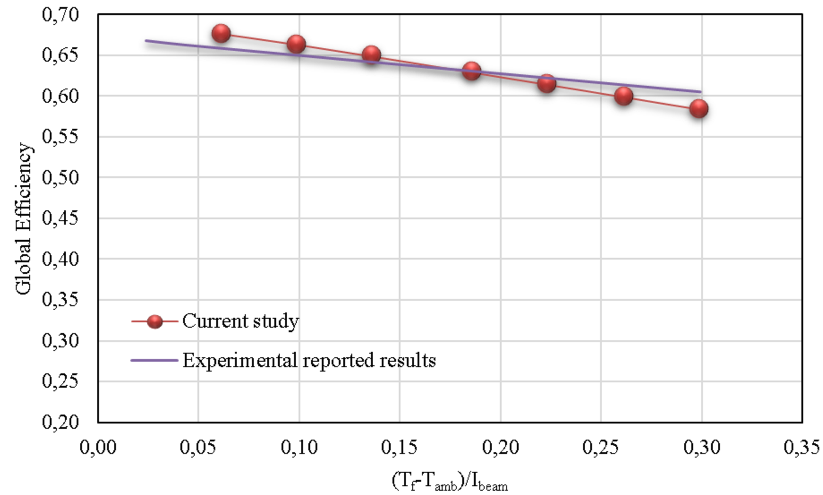

Figure 11: Comparison between the experimentally measured results by Ref. [44] and the calculated numerical results in this research.

3 Results and Discussion

3.1 Sensitivity Analysis

The first part of the results section is devoted to presenting the impact of the optical errors on the PTC performance. The results of this section correspond to the presented geometry with the values of Table 1. Figure 12 and Figure 13 illustrate the optical analysis results with the SolTrace software. In this analysis, the parameter "a" is assumed equal to the glass cover diameter. Practically, in this investigation, the position of the receiver changes and in every case a detailed optical analysis is conducted. Figure 12 depicts the optical analysis for the receiver while Figure 13 shows all the PTC system. In Figure 12 and Figure 13, the sub-Figure 12a and Figure 13a show the case with the receiver lower than the focal distance, the sub-Figure 12b and Figure 13b show the receiver in the focal distance and lastly the sub-Figure 12c and Figure 13c illustrate the receiver over the focal distance.

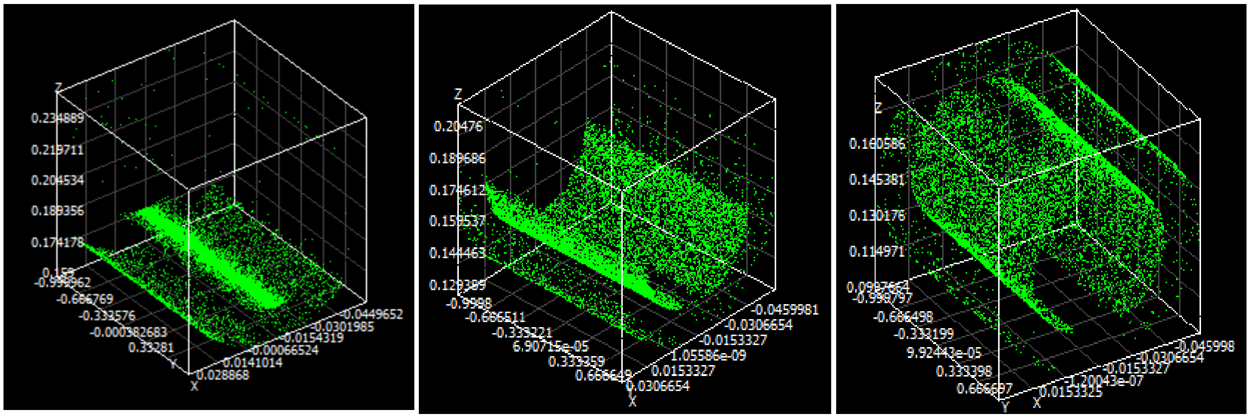

(a) **(b)** **(c)**

Figure 12: Optical analysis results of the receiver for the different receiver distances from the focal point a) [–a/2] b) [0] c) [a].

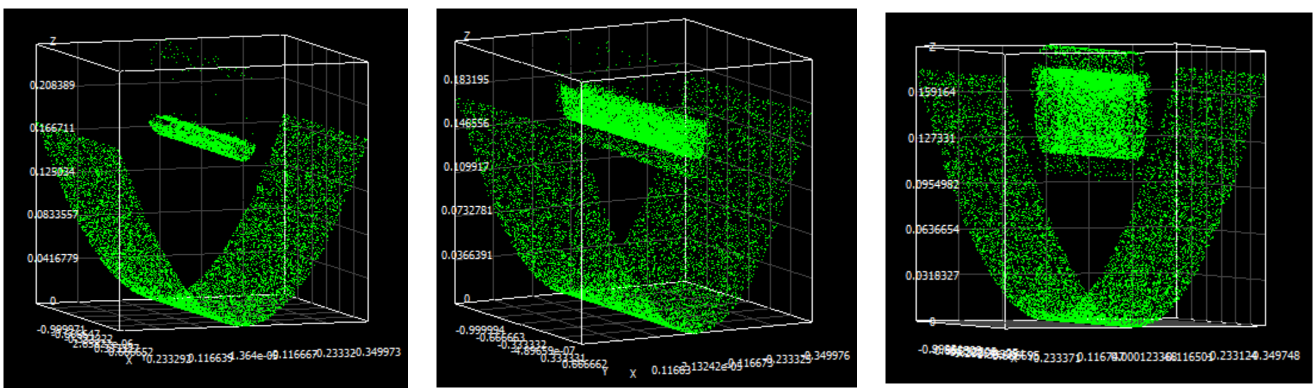

(a) **(b)** **(c)**

Figure 13: Optical analysis results of the solar PTC system for the different receiver distances from the focal point a) [–a/2] b) [0] c) [a].

Figure 14 and Figure 15 indicate the impact of the tracing error on the absorbed solar energy and on the optical efficiency respectively. It can be said that the maximum performance is found for zero tracking error and for the receiver at the focal point. Generally, the maximum optical efficiency is around 85% and it decreases to 75% when the receiver is located 0.03 m far from the focal point in the vertical direction. The maximum absorbed energy is around 1100 W for the receiver at the focal point, while the different errors can reduce it to 1060. For the case with the receiver at 0.03 m far from the focal point, the maximum absorbed energy is 958 W and the minimum 727 W.

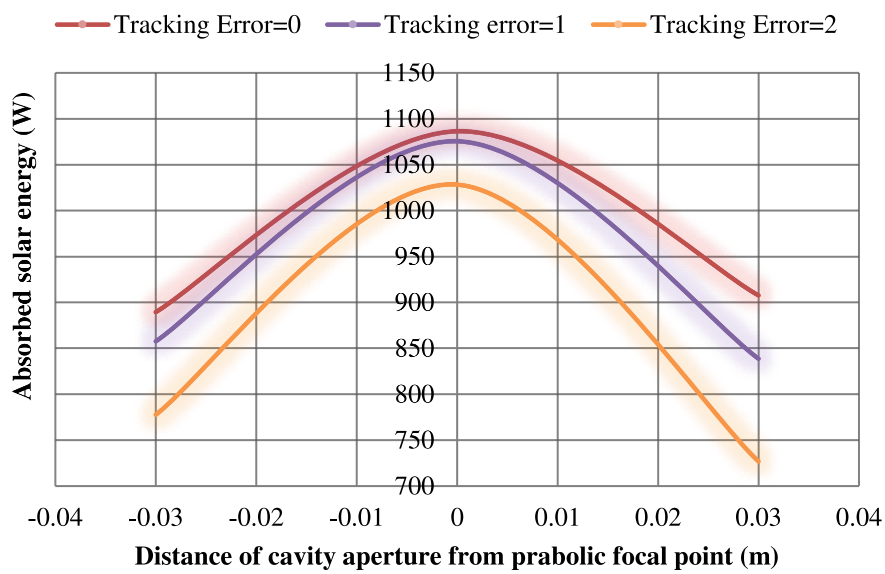

Figure 14: Absorbed solar energy variation versus different position of receiver compared to the focal point at different tracking error and optical error of 10 mrad.

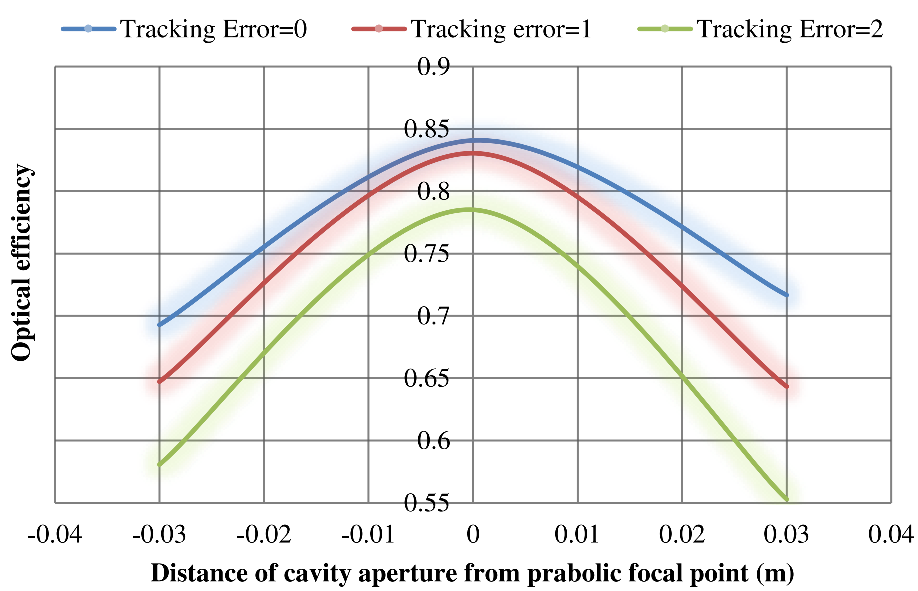

Figure 15: Optical efficiency variation versus different position of receiver compared to the focal point at different tracking error, and optical error of 10 mrad.

The results of the previous paragraphs proved that the optimum location of the receiver is found at the focal point. This section tries to determine the optimum receiver diameter for the examined PTC. Figure 16 and Figure 17 show the optical performance of the examined PTC for the different tube diameters and optical errors, while the Figure 18 indicates the thermal performance of the PTC for the different tube diameters and optical errors. Figure 16 shows the optical efficiency of the PTC for the different tube diameters. These results correspond to optical errors from 5 mrad up to 35 mrad with zero tracking error. It is obvious that the tube diameter has to be at least 0.02 m, in order to have an adequate optical efficiency for low optical errors. For higher optical errors, the tube diameter has to be greater and about 0.05 m, in order to absorb high amounts of solar irradiation. Similar results are found in Figure 17 for different tracking errors. Generally, a minimum diameter of 0.02 m is required for a satisfying optical performance when there is no tracking error. Higher diameters about 0.04 m are required for greater tracking errors.

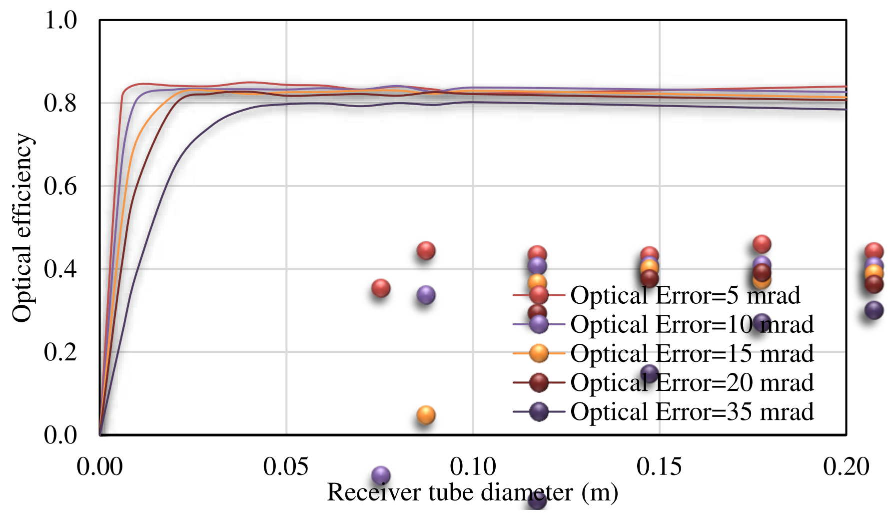

Figure 16: Variation of receiver tube versus different receiver tube diameters for different optical error at tracking error of 0 degrees.

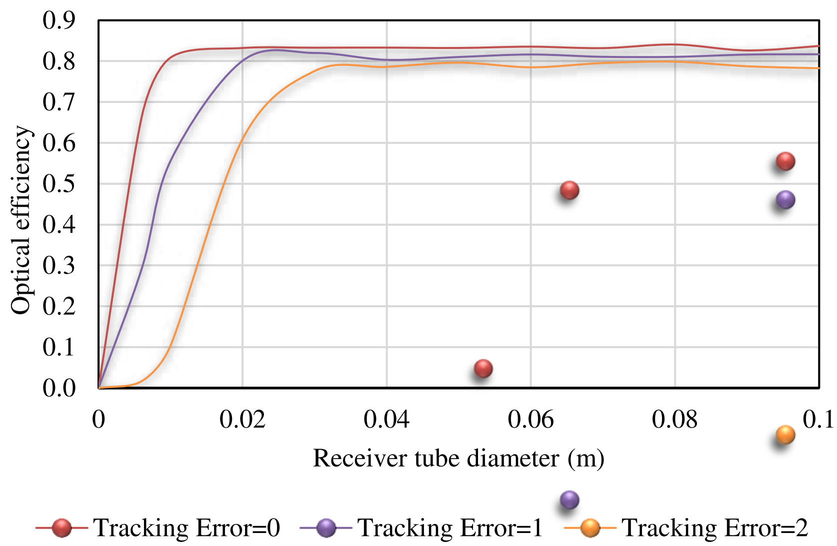

Figure 17: Variation of optical efficiency versus different receiver tube diameters for different tracking error at the optical error of 10 mrad.

Figure 18 shows the useful heat production and the receiver thermal efficiency for different tube diameters and optical errors. Figure 19 shows the useful heat production of and the receiver thermal efficiency for different tube diameters and tracking errors. It is obvious that the optimum tube diameter thermally is approximately equal to the minimum tube diameter which leads to maximum optical efficiency. In other words, the optimum tube diameter thermally needs high absorbed energy and a relatively low outer surface in order to reduce the thermal losses. The receiver efficiency is 81.3% for 5 mrad optical error, zero tracking error, while figure 20 shows maximum receiver efficiency at 76.6% for 10 mrad optical error and zero tracking error.

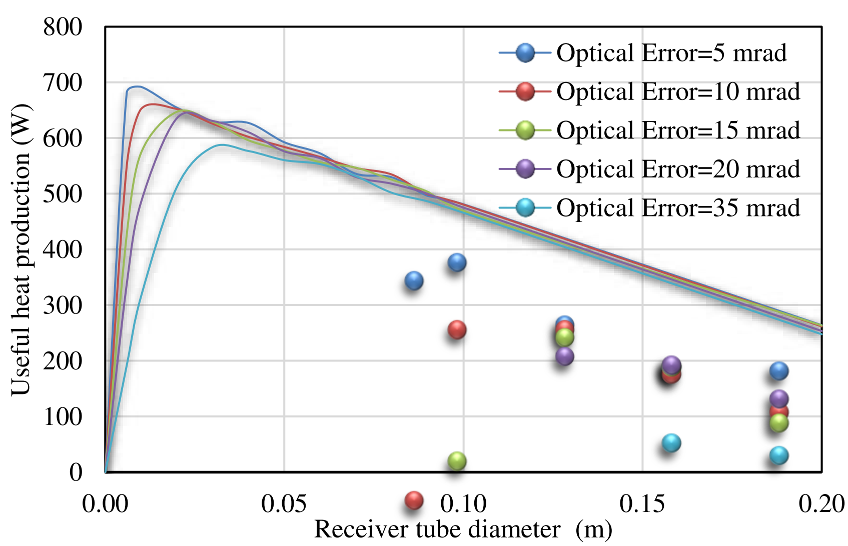

(a)

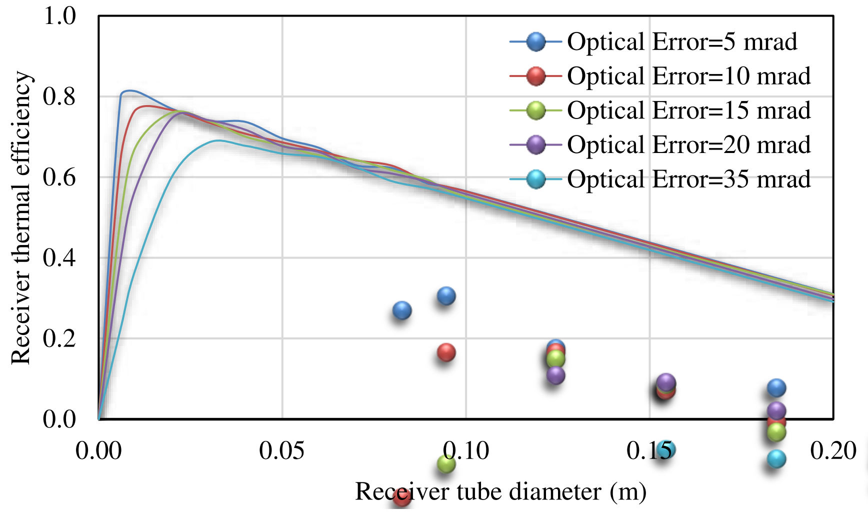

(b)

Figure 18: Variation of a) useful heat production, and b) thermal efficiency versus different receiver tube diameters for different optical error at tracking error of 0 degrees.

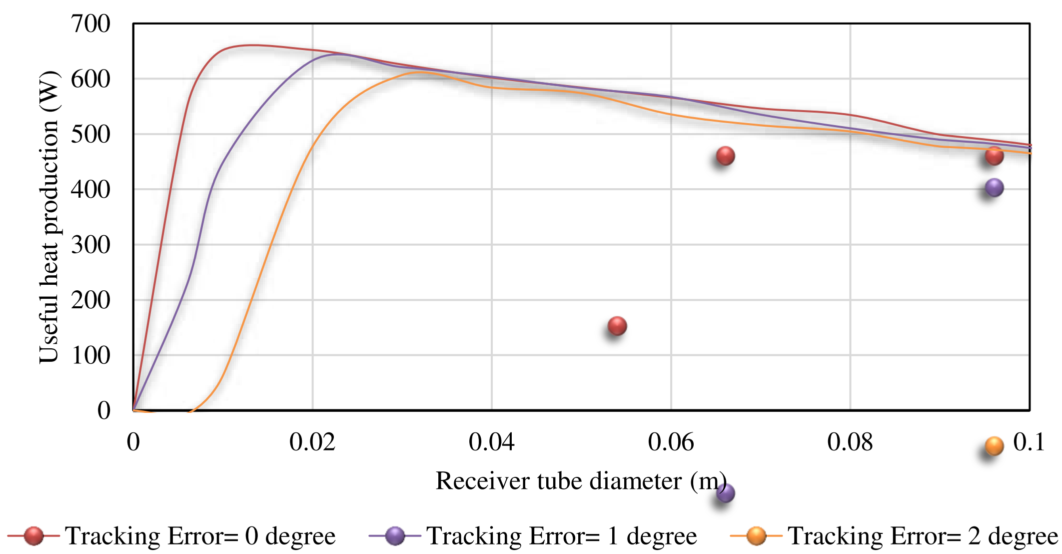

(a)

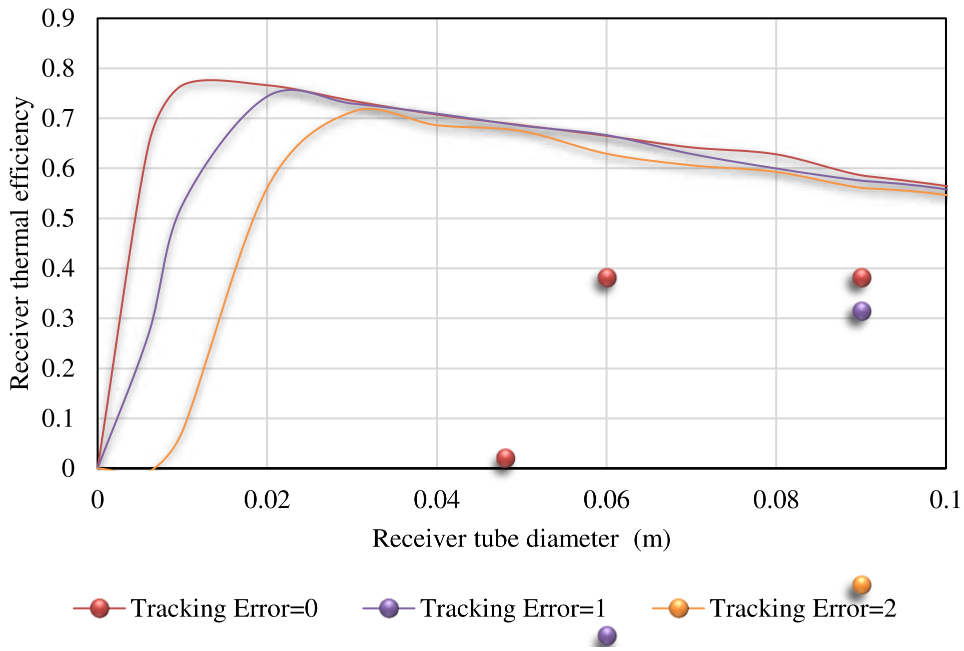

(b)

Figure 19: Variation of a) useful heat production, and b) thermal efficiency versus different receiver tube diameters for different tracking error at the optical error of 10 mrad.

3.2 Energy Analysis

In this section energy performance of the solar power system based on three suggested scenarios will be presented. It should be mentioned that all of these analyses were conducted for the calculated optimum diameter of the receiver tube as 20 mm, with PTC aperture area of 2×0.7 m^2. Also, constant conditions were assumed for analyses of the solar system including solar irradiance of 600 W/m^2, ambient temperature of 20ºC, oil inlet temperature of 50ºC, and oil flow rate of 50 ml/s. As stated, Behran thermal oil was used as the heat transfer fluid in the solar system.

3.2.1 SRC System

Variation of SRC net work, and SRC total efficiency with variation of TIT is presented in Figure 20a, and 20b, respectively. Values of TIT were varied between 507 K to 1200 K. Influence of five levels of condenser temperature was investigated on net work, and total efficiency of the solar SRC system including 30ºC, 35ºC, 40ºC, 45ºC, and 50ºC. It can be concluded from Figure 20 that amounts of net work, and total efficiency of the solar SRC system increased with increasing TIT, and decreasing condenser temperature. In another word, the highest values of net work, and total efficiency of the solar SRC system were calculated as 260.8 W, and 31.05% for TIT of 1200

K, and condenser temperature of 30ºC, respectively. As seen, net work, and total efficiency of the solar SRC system have a similar trend of data with variation of TIT. Consequently for achieving higher energy performance of the solar SRC system, higher amounts of TIT, and lower amounts of condenser temperature are recommended.

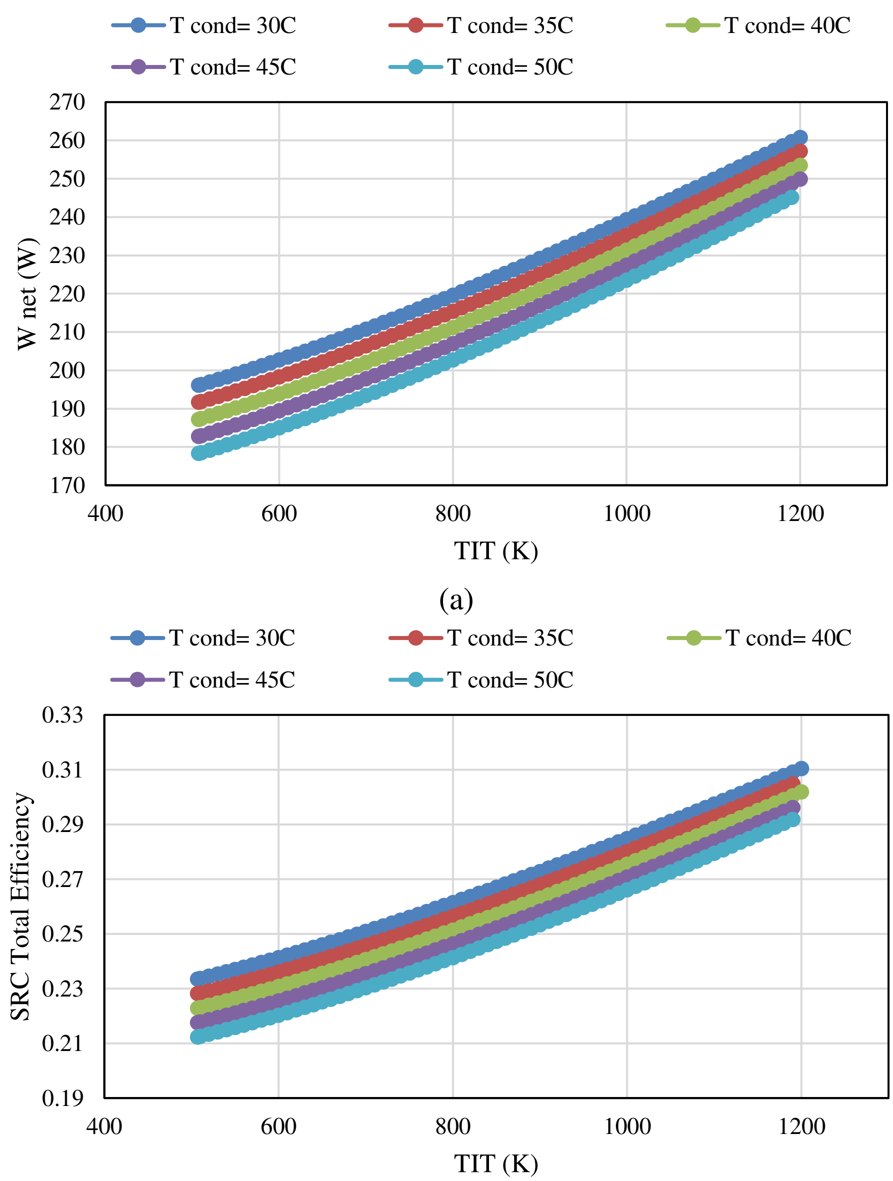

(b)

Figure 20: Variation of a) SRC net work, and b) SRC total efficiency with variation of TIT for five levels of condenser temperature.

Figure 21 presents variation of condenser ejected heat with variation of TIT for five levels of condenser temperature. It should be stated that TIT was changed in the range of 507 K to 1200 K, whereas condenser temperature was investigated at 30ºC, 35ºC, 40ºC, 45ºC, and 50ºC. As seen on Figure 21, amounts of the condenser ejected heat decreased with increasing TIT, and decreasing condenser temperature. The lowest condenser ejected heat was calculated equal to 296.89 W for TIT of 1200 K, and condenser temperature of 30ºC. Generally, lower amounts of condenser ejected heat are recommended for generation higher amounts of power.

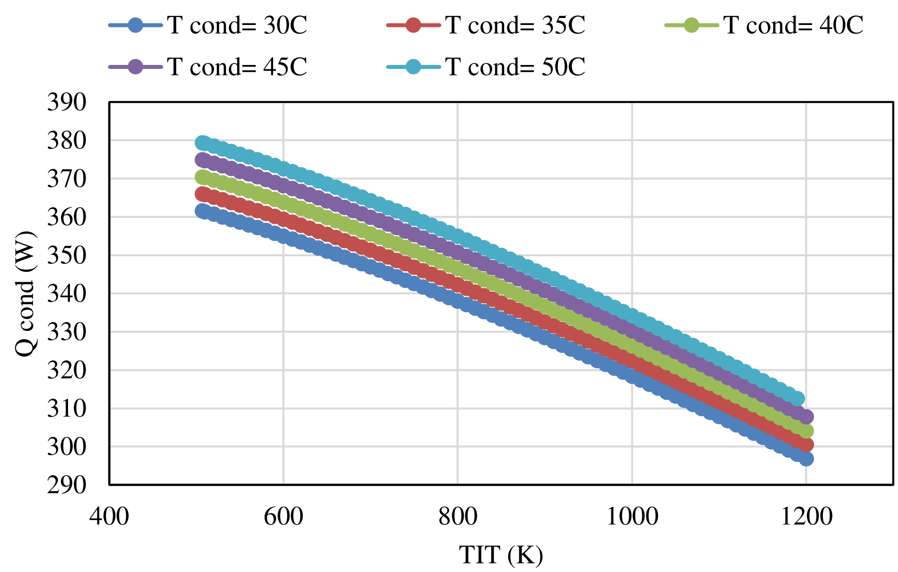

Figure 21: Variation of condenser ejected heat with variation of TIT for five levels of condenser temperature.

3.2.2 ORC System

In this part, energy performance of the solar ORC system will be reported. R113 was used as the ORC working fluid. Figure 22a, and 22b display variation of net work, and total efficiency with variation of TIT for five levels of the condenser temperature including 30ºC, 35ºC, 40ºC, 45ºC, and 50ºC, respectively. It should be noted that TIT was evaluated from 479 K to 524 K. As seen, lower amounts of the condenser temperature had resulted higher amounts of the net work, and total efficiency of the solar ORC system. On the other side, there are optimum amounts of the net work, and total efficiency with variation of TIT for each levels of the investigated condenser temperature. In other words, the highest amounts of the net work, and total efficiency were calculated at the TIT of 499 K for each levels of condenser temperatures. The highest amount of net work, and total efficiency were estimated equal to 148.18 W, and 17.64% for condenser temperature of 30ºC, and TIT of 499K, respectively. Also, similar trend of data can be seen between net work, and total efficiency of the solar ORC system with variation of TIT.

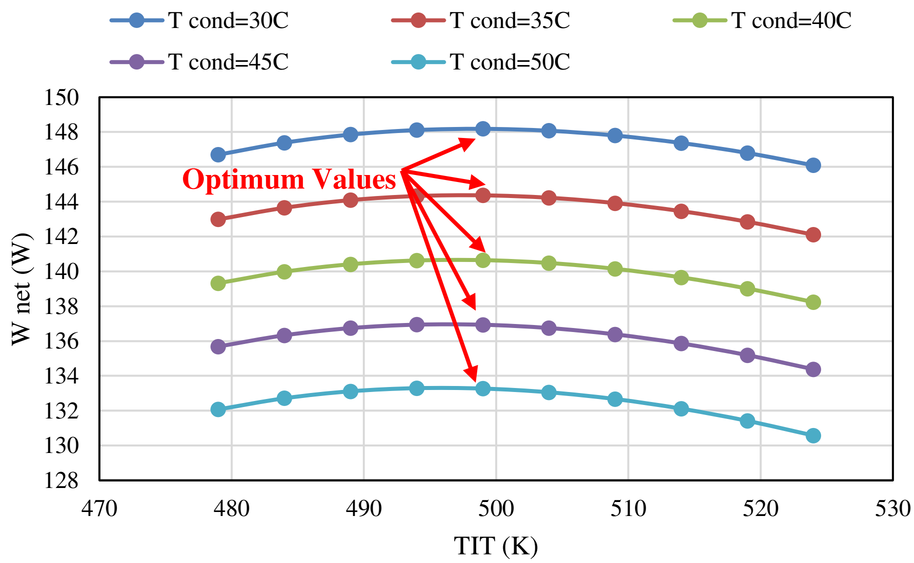

(a)

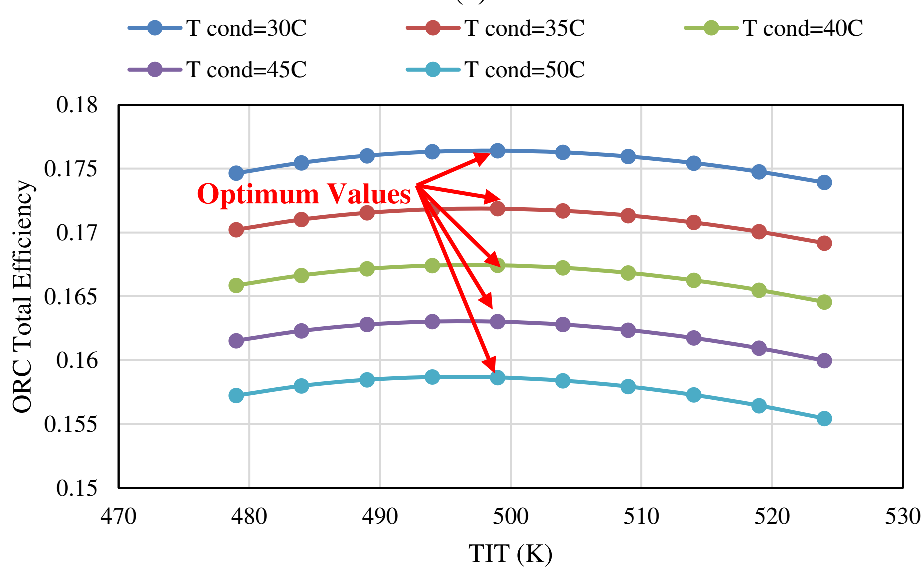

(b)

Figure 22: Variation of a) ORC net work, and b) ORC total efficiency with variation of TIT for five levels of condenser temperature.

Variation of condenser ejected heat by the ORC system with variation of TIT for five levels of condenser temperature including 30ºC, 35ºC, 40ºC, 45ºC, and 50ºC, is depicted in Figure 23. It should be mentioned that TIT was varied from 479 K to 524 K. Also, R113 at constant evaporator temperature of 3 MPa was used as the ORC working fluid. As resulted from Figure 23, values of the condenser ejected heat decreased with increasing TIT. On the other side, there is an optimum value of TIT equal to 499 K for achieving the lowest amounts of the condenser ejected heat for each investigated levels of condenser temperature. In general, lower amounts of condenser ejected heat are recommended for generating higher amounts of power. The lowest condenser ejected heat was calculated equal to 409.51 W for TIT as 499 K, and condenser temperature as 30ºC.

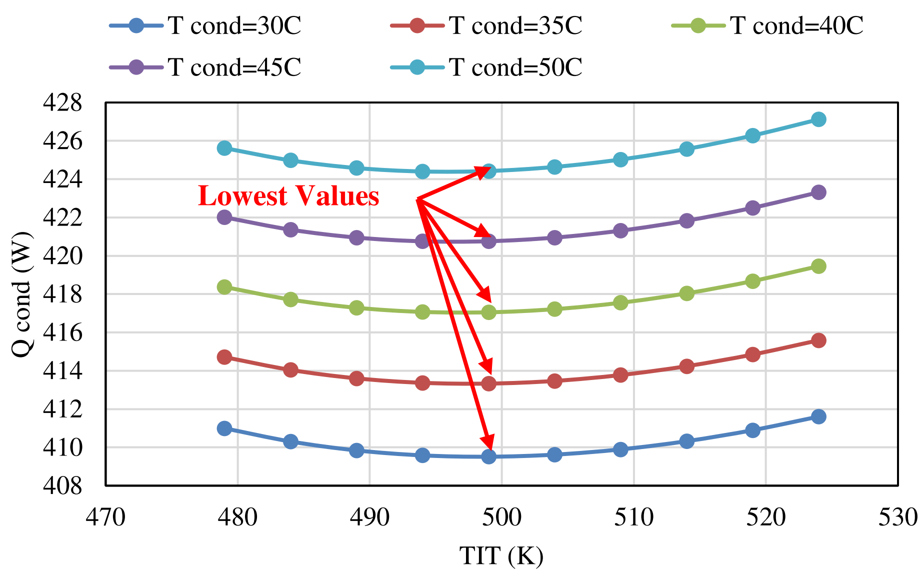

Figure 23: Variation of condenser ejected heat with variation of TIT for five levels of condenser temperature.

3.2.3 SRC+ORC System

In this part, energy performance of the solar power system based on the third scenario will be presented. As mentioned, a combination of SRC system, and ORC system was suggested as the third scenario. It should be mentioned that optimum condition of the SRC system including TIT of 1200 K, and condenser temperature of 30℃ was used as the first cycle, whereas the ejected heat by the SRC system was used as heat source of the ORC system as the second power cycle. It should be stated that the ORC system was evaluated with variation of TIT between 479 K to 524 K, and the condenser temperature at five levels including 30ºC, 35ºC, 40ºC, 45ºC, and 50ºC. R113 was used as the ORC working fluid. Figure 24a, and 24b present variation of net work, and total efficiency of the combined system with variation of TIT for five levels of the condenser temperature, respectively. As concluded from Figure 24, lower amounts of the condenser temperature had resulted higher amounts of the net work, and total efficiency of the combined solar SRC+ORC system. On the other hand, there are optimum amounts of the net work, and total efficiency with variation of TIT for each five levels of the investigated condenser temperature. The highest amounts of the net work, and total efficiency were calculated at the TIT of 499 K for each levels of condenser temperatures. The highest amount of net work, and total efficiency were estimated equal to 339.69 W, and 40.44% for condenser temperature of 30ºC, and TIT of 499K, respectively. As resulted, amounts of net work, and total efficiency of the combined solar SRC+ORC system had significantly increased compared to individual solar SRC system, and solar ORC system as presented in the previous sections. Concluded, the combined solar SRC+ORC system is recommended for achieving higher amounts of net work, and total efficiency.

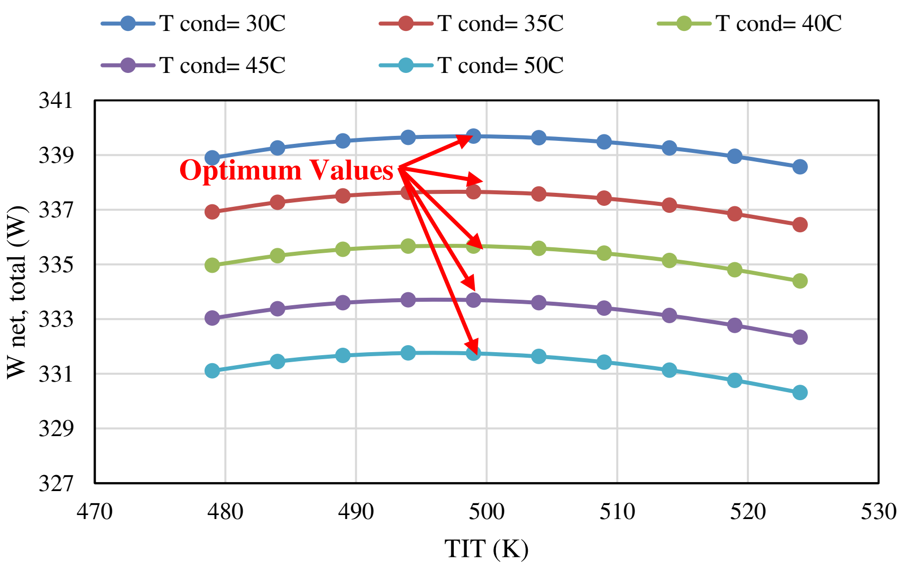

(a)

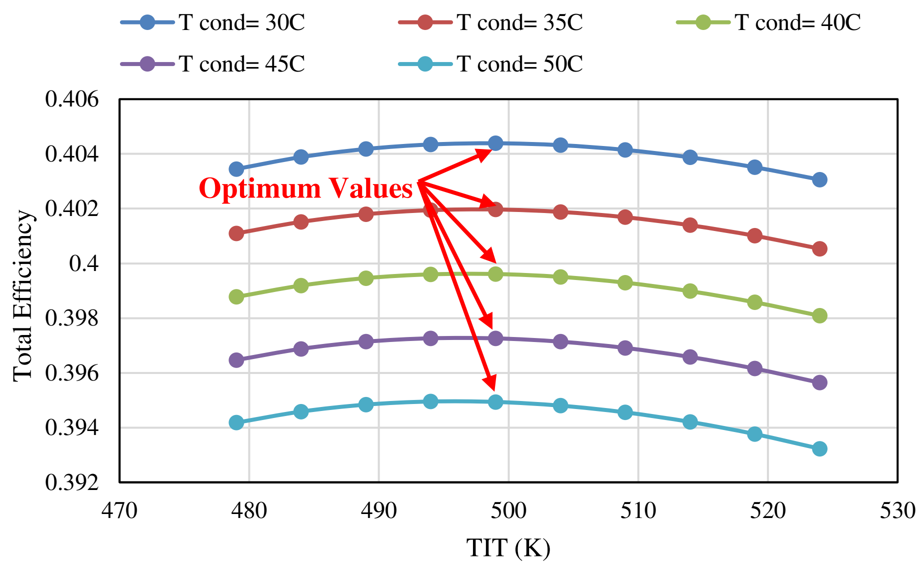

(b)

Figure 24: Variation of a) SRC+ORC net work, and b) SRC+ORC total efficiency with variation of TIT for five levels of condenser temperature.

Figure 25 depicts variation of condenser ejected heat by the combined SRC+ORC system with variation of TIT from 479 K to 524 K. Five levels of condenser temperature including 30ºC, 35ºC, 40ºC, 45ºC, and 50ºC, were investigated. As mentioned R113 at constant evaporator temperature of 3 MPa was used as the ORC working fluid. Optimum condition of the SRC system was investigated including TIT of 1200 K, and condenser temperature of 30℃. As seen, there is an optimum TIT as 499 K for achieving the lowest amounts of the condenser ejected heat for each investigated levels of condenser temperature. Mainly, lower amounts of condenser ejected heat are recommended for generating higher amounts of power. On the other side, the condenser ejected heat decreased with increasing TIT. The lowest condenser ejected heat of the combined solar SRC+ORC system was calculated equal to 218 W for TIT as 499 K, and condenser temperature as 30ºC.

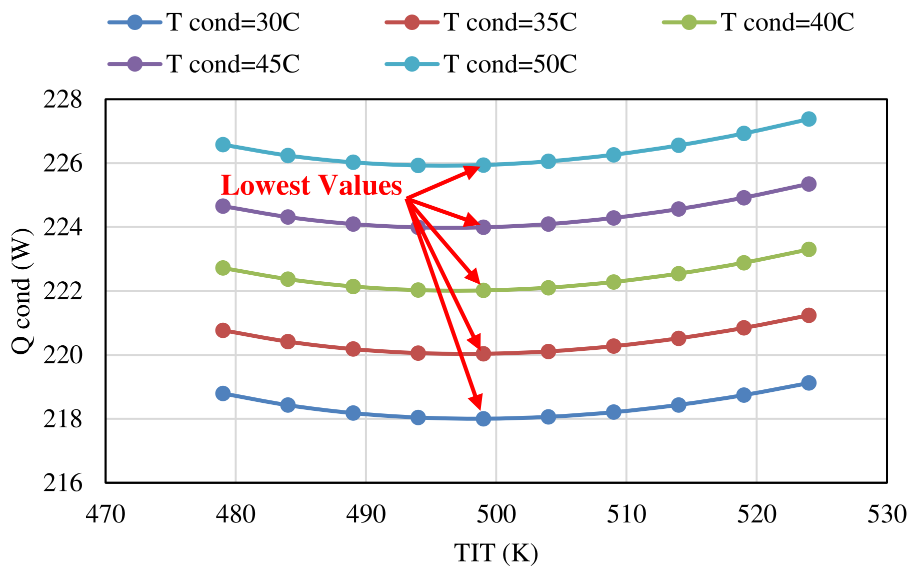

Figure 25 Variation of condenser ejected heat with variation of TIT for five levels of condenser temperature.

3.3 Exergy Analysis

In this part, exergy analysis of the solar power system will be reported based on three suggested scenarios including solar SRC system, solar ORC system, and solar SRC+ORC system. It should be stated that all of these analyses were conducted for the calculated optimum receiver diameter of 20 mm, with PTC aperture area of 2×0.7 m^2. Also, Behran thermal oil was used as the heat transfer fluid in the solar system. On the other side, all of the analyses were conducted under constant conditions of the solar system including solar irradiance of 600 W/m^2, ambient temperature of 20ºC, oil inlet temperature of 50ºC, and oil flow rate of 50 ml/s.

3.3.1 SRC System

Variation of exergy electrical efficiency with variation of TIT plots on Figure 26. Five levels of condenser temperature was investigated on the exergy electrical efficiency of the solar SRC system including 30ºC, 35ºC, 40ºC, 45ºC, and 50ºC. It should be mentioned that TIT were varied from 507 K to 1200 K, whereas evaporator pressure was assumed as a constant value of 3MPa. It can be resulted from Figure 26 that amounts of exergy electrical efficiency of the solar SRC system improved with increasing TIT, and decreasing condenser temperature. The highest value of exergy electrical efficiency of the solar SRC system was calculated as 33.30% for TIT of

1200 K, and condenser temperature of 30ºC. Consequently for achieving higher exergy electrical efficiency of the solar SRC system, higher amounts of TIT, and lower amounts of condenser temperature are recommended.

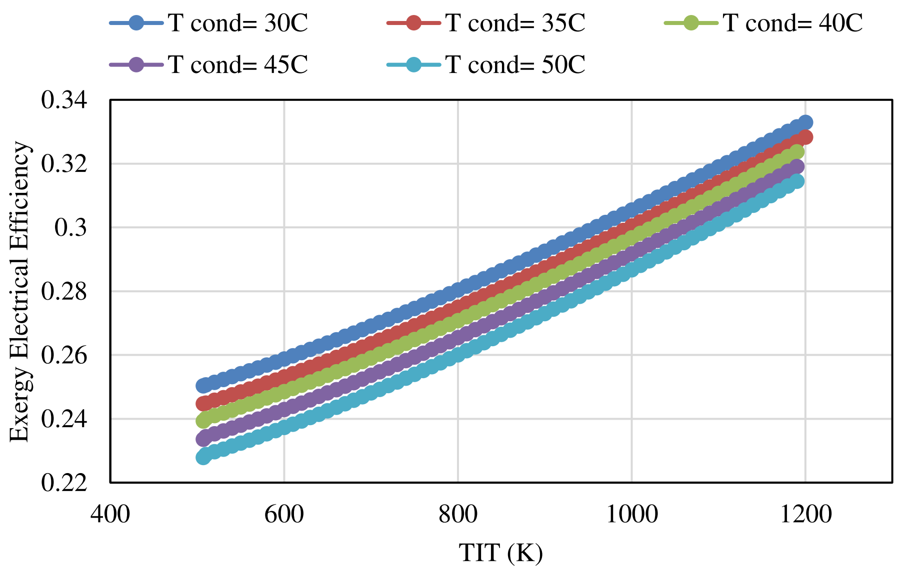

Figure 26: Variation of SRC exergy electrical efficiency with variation of TIT for five levels of condenser temperature.

3.3.2 ORC System

Variation of exergy electrical efficiency with variation of TIT is presented in Figure 27 for five levels of the condenser temperature including 30ºC, 35ºC, 40ºC, 45ºC, and 50ºC. As stated, R113 was used as the ORC working fluid. TIT of the ORC system was changed from 479 K to 524 K. As concluded, lower amounts of the condenser temperature had resulted higher amounts of exergy electrical efficiency of the solar ORC system. On the other side, there are optimum amounts of exergy electrical efficiency with variation of TIT for each level of the condenser temperature. In other words, the highest exergy electrical efficiency was calculated at the TIT of 499 K for each levels of condenser temperatures. The highest exergy electrical efficiency was calculated equal to 18.91% for condenser temperature of 30ºC, and TIT of 499K.

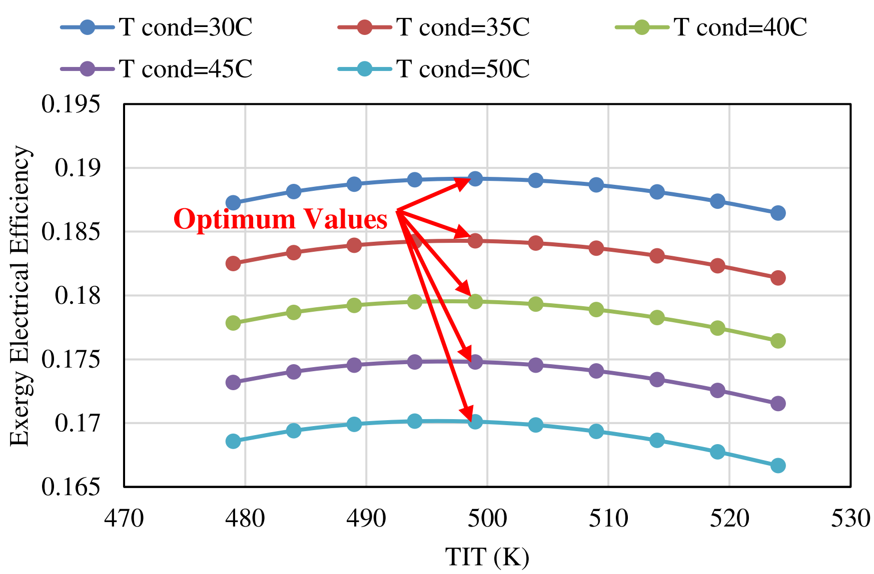

Figure 27: Variation of ORC exergy electrical efficiency with variation of TIT for five levels of condenser temperature.

3.3.3 SRC+ORC System

Exergy electrical efficiency of the solar combined SRC+ORC system based on the third assumed scenario will be reported. As mentioned, optimum condition of the SRC system including TIT of 1200 K, and condenser temperature of 30°C was used as the first cycle, whereas the ejected heat by the SRC system was used as heat source of the ORC system as the second power cycle. The ORC system was considered with variation of TIT from 479 K to 524 K, and five levels of the condenser temperature including 30ºC, 35ºC, 40ºC, 45ºC, and 50ºC. Also, R113 at constant evaporator pressure of 3 MPa was used as the ORC working fluid. Variation of exergy electrical efficiency of the combined SRC+ORC system with variation of TIT for five levels of the condenser temperature is presented in Figure 28. As concluded from Figure 28, lower amounts of the condenser temperature concluded higher amounts of the exergy electrical efficiency. On the other side, there are optimum amounts of exergy electrical efficiency with variation of TIT for each five levels of the investigated condenser temperature. The highest value of exergy electrical efficiency was calculated as 43.36% for condenser temperature of 30ºC, and TIT of 499K. As seen, exergy electrical efficiency of the combined solar SRC+ORC system had significantly improved compared to individual solar SRC system, and solar ORC system as reported in the previous sections. So, the combined solar SRC+ORC system is recommended for achieving higher exergy electrical efficiency.

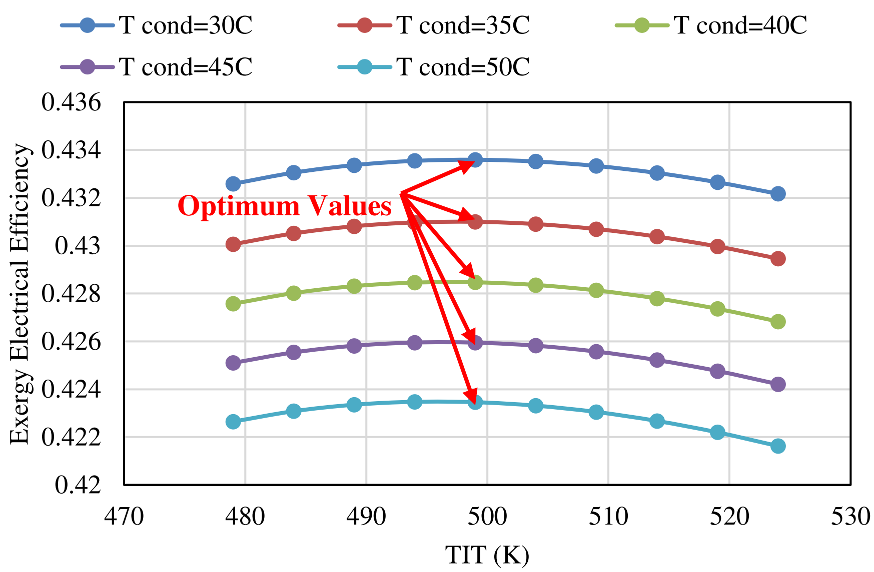

Figure 28: Variation of SRC+ORC exergy electrical efficiency with variation of TIT for five levels of condenser temperature.

3.4 Economic Analysis

In this section, economic analysis of three suggested scenarios for generation power will be presented. Table 4 reports economic analysis of three suggested scenarios. It should be noted that optimized conditions of three suggested scenarios were assumed for achieving the highest energy and exergy performance based on the previous sections. In other words, the optimized conditions that were used in this section are including the PTC receiver diameter as 20 mm, PTC aperture area as 2×0.7 m^2, condenser temperature as 30ºC, TIT as 1200 K for SRC system, and TIT as 499 K for ORC system. The total energy efficiency of the solar SRC system, solar ORC system, and solar combined SRC+ORC system of the assumed systems in this section were calculated equal to 31.05%, 17.64%, and 40.49%, respectively. Whereas, the exergy electrical efficiency of the solar SRC system, solar ORC system, and solar combined SRC+ORC system of the assumed systems in this part were as 33.29%, 18.91%, and 43.36%, respectively. It should be mentioned that all of the reported economic results are based on providing 2700 W/day for the suggested mobile house in section 2.1. As seen in Table 4, the third assumed scenario had shown the lowest amount of Simple Payback Period (SPP) as about 6.57 years, the highest Cash Flow (CF) amount as 195.81 €/year, and the lowest Levelized Cost of Electricity (LCOE) as 0.0535 €/kWh. In other hand, total cost of the solar combined SRC+ORC system for providing the required power of the suggested mobile house was estimated as the lowest value equal to 1285.73 €/unit among the other studied scenarios. Consequently, providing the required power of the suggested mobile house by the solar combined SRC+ORC system is recommended due to the best economic performance among the other investigated scenarios.

Table 4: Economic analysis of three suggested scenarios.

Scenario	$\dot{W}_{net}$ (W)	$\dot{W}_{net}$ (Wh/day)	LCOE (€/kWh)	CF (€/year)	SPP (years)	$Cost_{total}$ (€/unit)
SRC	260.80	2086.44	0.0569	195.73	6.99	1368.37
ORC	148.18	1185.47	0.0682	195.46	8.38	1638.83
SRC+ORC	339.69	2717.52	0.0535	195.81	6.57	1285.73

3.1 Environmental Analysis

Environmental analysis of three suggested scenarios based on the optimized conditions as presented in the previous section will be presented. Environmental analysis of three suggested scenarios is reported in Table 5. As mentioned the assumed conditions are including the PTC receiver diameter as 20 mm, PTC aperture area as 2×0.7 m^2, condenser temperature as 30ºC, TIT as 1200 K for SRC system, and TIT as 499 K for ORC system. It should be stated that all of the reported environmental results are based on providing 2700 W/day for the suggested mobile house in section 2.1. As concluded from Table 5, the CO_2 mitigated per annum (φ_{CO_2}) was estimated about 5.29 (tone /year), and the carbon credit (Z_{CO_2}) was calculated equal to 76.71 ($/year). As seen, application of the suggested solar power system additional to providing required power in natural disasters such as Kermanshah earthquake on 2016, has positive influence on environmental condition for reducing CO_2 emission.

Table 5: Environmental analysis of three suggested scenarios.

$\dot{W}_{net}$ (kWh/year)	φ_{CO_2} $(tone$ /year)	Z_{CO_2} ($/year)
985.50	5.29	76.71

3.2 Summation of Analyses for Kermanshah Earthquake

Based on the done 4E analyses for providing required power of a mobile house in natural disasters such as Kermanshah earthquake on 2016, the optimized solar power system was determined using the following characteristics:

- System type: solar combined SRC+ORC system,
- PTC receiver diameter: 20 mm,
- PTC aperture area: 2×0.7 m^2,
- Condenser temperature: 30ºC,
- TIT of the SRC system: 1200 K,
- TIT of ORC system: 499 K,
- Total energy efficiency: 40.49%,
- Exergy electrical efficiency: 43.36%,
- Simple Payback Period (SPP): 6.57 years,
- Cash Flow (CF): 195.81 €/year,
- Levelized Cost of Electricity (LCOE): 0.0535 €/kWh,
- Total cost: 1285.73 €/unit
- CO_2 mitigated per annum (φ_{CO_2}): 5.29 (tone /year),
- Carbon credit (Z_{CO_2}): 76.71 ($/year).

Finally, it can be concluded that for each 10000 homeless, if each family was assumed as 5 persons, about 2.571 million € needs for providing power of the designed mobile house.

4 Conclusions

In the current research, different configurations of solar Rankine cycles for power generation of a mobile-house in emergency condition such as earthquake were investigated. Different configurations of the power generation systems were including solar Steam Rankine Cycle (SRC), solar Organic Rankine Cycle (ORC), and solar SRC-ORC system. The solar systems were evaluated based on 4E analyses including energy (E1), exergy (E2), environmental (E3), and economic (E4). Solar Parabolic Trough Concentrators (PTCs) were evaluated as heat source of the power generation systems. The main subject of this study is designing a mobile-house for providing required power of homeless people in natural disasters such as earthquake that was happened in Kermanshah, Iran, on 2016. The most important conclusions of this study are summarized below:

- The optimum location for the PTC receiver is at the focal point. Moreover, the optimum receiver is around 0.02 m for the design with low errors, while it is up to 0.04 m for greater errors.

- The maximum optical efficiency is around 85% while the maximum thermal efficiency is around 81%.

- The decrease of the optical and thermal efficiency with the optical/tracking errors is more intense for the cases with a displaced receiver.

- It was concluded that the combined solar SRC+ORC system can be recommended for achieving the highest amounts of net work, and total efficiency as 339.69 W, and 40.44% for condenser temperature of 30ºC, and TIT of 499K, respectively.

- The combined solar SRC+ORC system is recommended for achieving higher exergy electrical efficiency as 43.36% for condenser temperature of 30ºC, and TIT of 499K.

- The combined solar SRC+ORC system assumed scenario had shown the lowest amount of Simple Payback Period (SPP) as about 6.57 years, the highest Cash Flow (CF) amount as 195.81 €/year, and the lowest Levelized Cost of Electricity (LCOE) as 0.0535 €/kWh.

- The CO_2 mitigated per annum (φ_{CO_2}) was estimated about 5.29 (tone /year), and the carbon credit (Z_{CO_2}) was calculated equal to 76.71 ($/year).

Acknowledgement

Dr. Loni, and Dr. Najafi are grateful to the Tarbiat Modares University (http://www.modares.ac.ir) for financial supports given under IG/39705 grant for renewable Energies of Modares research group.

References

[1] P. Devine-Wright, Place attachment and public acceptance of renewable energy: A tidal energy case study, Journal of Environmental Psychology, 31 (2011) 336-343.

[2] J.P.C. Bento, V. Moutinho, CO2 emissions, non-renewable and renewable electricity production, economic growth, and international trade in Italy, Renewable and Sustainable Energy Reviews, 55 (2016) 142-155.

[3] A. Assali, T. Khatib, A. Najjar, Renewable energy awareness among future generation of Palestine, Renewable Energy, (2019).

[4] R. Loni, A. Kasaeian, E.A. Asli-Ardeh, B. Ghobadian, Optimizing the efficiency of a solar receiver with tubular cylindrical cavity for a solar-powered organic Rankine cycle, Energy, 112 (2016) 1259-1272.

[5] J. Song, K. Tong, L. Li, G. Luo, L. Yang, J. Zhao, A tool for fast flux distribution calculation of parabolic trough solar concentrators, Solar Energy, 173 (2018) 291-303.

[6] O. Jaramillo, E. Venegas-Reyes, J. Aguilar, R. Castrejón-García, F. Sosa-Montemayor, Parabolic trough concentrators for low enthalpy processes, Renewable Energy, 60 (2013) 529-539.

[7] E. Bellos, C. Tzivanidis, Alternative designs of parabolic trough solar collectors, Progress in Energy and Combustion Science, 71 (2019) 81-117.

[8] D. Azzouzi, H. eddine Bourorga, K. abdelrahim Belainine, B. Boumeddane, Experimental study of a designed solar parabolic trough with large rim angle, Renewable Energy, 125 (2018) 495-500.

[9] S. Khanna, V. Sharma, S. Newar, T.K. Mallick, P.K. Panigrahi, Thermal stress in bimetallic receiver of solar parabolic trough concentrator induced due to non uniform temperature and solar flux distribution, Solar Energy, 176 (2018) 301-311.

[10] U. Caldiño-Herrera, L. Castro, O. Jaramillo, J. Garcia, G. Urquiza, F. Flores, Small Organic Rankine Cycle Coupled to Parabolic Trough Solar Concentrator, Energy Procedia, 129 (2017) 700-707.

[11] M. Wirz, J. Petit, A. Haselbacher, A. Steinfeld, Potential improvements in the optical and thermal efficiencies of parabolic trough concentrators, Solar Energy, 107 (2014) 398-414.

[12] I. Karathanassis, E. Papanicolaou, V. Belessiotis, G. Bergeles, Design and experimental evaluation of a parabolic-trough concentrating photovoltaic/thermal (CPVT) system with high-efficiency cooling, Renewable Energy, 101 (2017) 467-483.

[13] S. Srivastava, K. Reddy, Simulation studies of thermal and electrical performance of solar linear parabolic trough concentrating photovoltaic system, Solar Energy, 149 (2017) 195-213.

[14] N. Kincaid, G. Mungas, N. Kramer, M. Wagner, G. Zhu, An optical performance comparison of three concentrating solar power collector designs in linear Fresnel, parabolic trough, and central receiver, Applied Energy, 231 (2018) 1109-1121.

[15] M. Reyes-Belmonte, A. Sebastián, J. Spelling, M. Romero, J. González-Aguilar, Annual performance of subcritical Rankine cycle coupled to an innovative particle receiver solar power plant, Renewable energy, 130 (2019) 786-795.

[16] N.B. Desai, S. Bandyopadhyay, Thermo-economic comparisons between solar steam Rankine and organic Rankine cycles, Applied Thermal Engineering, 105 (2016) 862-875.

[17] I. Dincer, M.E. Demir, 4.8 Steam and Organic Rankine Cycles, (2018).

[18] O. Aboelwafa, S.-E.K. Fateen, A. Soliman, I.M. Ismail, A review on solar Rankine cycles: Working fluids, applications, and cycle modifications, Renewable and Sustainable Energy Reviews, 82 (2018) 868-885.

[19] P. Garg, K. Srinivasan, P. Dutta, P. Kumar, Comparison of CO2 and steam in transcritical Rankine cycles for concentrated solar power, Energy procedia, 49 (2014) 1138-1146.

[20] V. Cheang, R. Hedderwick, C. McGregor, Benchmarking supercritical carbon dioxide cycles against steam Rankine cycles for concentrated solar power, Solar Energy, 113 (2015) 199-211.

[21] J. Li, P. Li, G. Pei, J.Z. Alvi, J. Ji, Analysis of a novel solar electricity generation system using cascade Rankine cycle and steam screw expander, Applied Energy, 165 (2016) 627-638.

[22] P. Li, J. Li, G. Gao, G. Pei, Y. Su, J. Ji, B. Ye, Modeling and optimization of solar-powered cascade Rankine cycle system with respect to the characteristics of steam screw expander, Renewable Energy, 112 (2017) 398-412.

[23] C. Sarmiento, J.M. Cardemil, A.J. Díaz, R. Barraza, Parametrized analysis of a Carbon Dioxide transcritical Rankine cycle driven by solar energy, Applied Thermal Engineering, (2018).

[24] P. Morrone, A. Algieri, T. Castiglione, Hybridisation of biomass and concentrated solar power systems in transcritical organic Rankine cycles: A micro combined heat and power application, Energy Conversion and Management, 180 (2019) 757-768.

[25] J.-L. Bouvier, G. Michaux, P. Salagnac, T. Kientz, D. Rochier, Experimental study of a micro combined heat and power system with a solar parabolic trough collector coupled to a steam Rankine cycle expander, Solar Energy, 134 (2016) 180-192.

[26] F. Carlson, J.H. Davidson, N. Tran, A. Stein, Model of the impact of use of thermal energy storage on operation of a nuclear power plant Rankine cycle, Energy Conversion and Management, 181 (2019) 36-47.

[27] U. Pelay, L. Luo, Y. Fan, D. Stitou, C. Castelain, Integration of a thermochemical energy storage system in a Rankine cycle driven by concentrating solar power: Energy and exergy analyses, Energy, 167 (2019) 498-510.

[28] K. Mohammadi, J.G. McGowan, Thermodynamic analysis of hybrid cycles based on a regenerative steam Rankine cycle for cogeneration and trigeneration, Energy Conversion and Management, 158 (2018) 460-475.

[29] S. Shaaban, Analysis of an integrated solar combined cycle with steam and organic Rankine cycles as bottoming cycles, Energy Conversion and Management, 126 (2016) 1003-1012.

[30] A.A. Shayesteh, O. Koohshekan, A. Ghasemi, M. Nemati, H. Mokhtari, Determination of the ORC-RO system optimum parameters based on 4E analysis; Water–Energy-Environment nexus, Energy Conversion and Management, 183 (2019) 772-790.

[31] J. Wang, Z. Lu, M. Li, N. Lior, W. Li, Energy, exergy, exergoeconomic and environmental (4E) analysis of a distributed generation solar-assisted CCHP (combined cooling, heating and power) gas turbine system, Energy, 175 (2019) 1246-1258.

[32] https://en.wikipedia.org/wiki/2017_Iran%E2%80%93Iraq_earthquake in.

[33] T. Sokhansefat, A. Kasaeian, F. Kowsary, Heat transfer enhancement in parabolic trough collector tube using Al2O3/synthetic oil nanofluid, Renewable and Sustainable Energy Reviews, 33 (2014) 636-644.

[34] W.G. Le Roux, T. Bello-Ochende, J.P. Meyer, The efficiency of an open-cavity tubular solar receiver for a small-scale solar thermal Brayton cycle, Energy Conversion and Management, 84 (2014) 457-470.

[35] A. Ratzel, C. Hickox, D. Gartling, Techniques for reducing thermal conduction and natural convection heat losses in annular receiver geometries, Journal of Heat Transfer, 101 (1979) 108-113.

[36] T.L. Bergman, F.P. Incropera, D.P. DeWitt, A.S. Lavine, Fundamentals of heat and mass transfer, John Wiley & Sons, 2011.

[37] S.W. Churchill, H.H. Chu, Correlating equations for laminar and turbulent free convection from a horizontal cylinder, International journal of heat and mass transfer, 18 (1975) 1049-1053.

[38] A. Žukauskas, Heat transfer from tubes in crossflow, in: Advances in heat transfer, Elsevier, 1972, pp. 93-160.

[39] Y.A. Cengel, A.J. Ghajar, M. Kanoglu, Heat and mass transfer: fundamentals & applications, McGraw-Hill New York, 2011.

[40] P. Berdahl, M. Martin, Emissivity of clear skies, Solar Energy, 32 (1984) 663-664.

[41] Y.A. Cengel, ThermodynamicsAn Engineering Approach 5th Edition By Yunus A Cengel: ThermodynamicsAn Engineering Approach, Digital Designs, 2011.

[42] L. Sahota, G. Tiwari, Exergoeconomic and enviroeconomic analyses of hybrid double slope solar still loaded with nanofluids, Energy Conversion and Management, 148 (2017) 413-430.

[43] E. Bellos, C. Tzivanidis, Assessment of linear solar concentrating technologies for Greek climate, Energy conversion and management, 171 (2018) 1502-1513.

[44] A. Kasaeian, S. Daviran, R.D. Azarian, A. Rashidi, Performance evaluation and nanofluid using capability study of a solar parabolic trough collector, Energy conversion and management, 89 (2015) 368-375.

[45] R. Loni, E.A. Asli-Ardeh, B. Ghobadian, A. Kasaeian, E. Bellos, Energy and exergy investigation of alumina/oil and silica/oil nanofluids in hemispherical cavity receiver: Experimental Study, Energy, 164 (2018) 275-287.